

# Towards a Re-evaluation of Data Forging Attacks in Practice

Mohamed Suliman<sup>1,2</sup> Anisa Halimi<sup>1</sup> Swanand Kadhe<sup>1</sup> Nathalie Baracaldo<sup>1</sup> Douglas Leith<sup>2</sup>

<sup>1</sup> IBM Research <sup>2</sup> Trinity College Dublin, The University of Dublin

**Abstract**—Data forging attacks provide counterfactual proof that a model was trained on a given dataset, when in fact, it was trained on another. These attacks work by forging (replacing) mini-batches with ones containing distinct training examples that produce nearly identical gradients. Data forging appears to break any potential avenues for data governance, as adversarial model owners may forge their training set from a dataset that is not compliant to one that is. Given these serious implications on data auditing and compliance, we critically analyse data forging from both a practical and theoretical point of view, finding that a key practical limitation of current attack methods makes them easily detectable by a verifier; namely that they cannot produce sufficiently identical gradients. Theoretically, we analyse the question of whether two distinct mini-batches can produce the same gradient. Generally, we find that while there may exist an infinite number of distinct mini-batches with real-valued training examples and labels that produce the same gradient, finding those that are within the allowed domain e.g. pixel values between 0-255 and one hot labels is a non trivial task. Our results call for the reevaluation of the strength of existing attacks, and for additional research into successful data forging, given the serious consequences it may have on machine learning and privacy.

## I. INTRODUCTION

Data governance is becoming an increasingly important subject with the rise of indiscriminate scraping of web data to train machine learning models. Legislation such as the GDPR Framework [25], [24] and the CCPA [15] have been introduced to prevent the use of potentially sensitive personal information during the training process and reduce potential harm to the data owners that may result from the proliferation of these models. Multiple stakeholders exist: data owners want assurances that their copyrighted or private information has not been used to train models without their consent, while the model owners want to prove that their training data is legally compliant.

Data forging [23], [12], [3], [29] has recently emerged as a new attack against machine learning models, particularly against data governance. Data forging attacks appear to provide counterfactual “proof” that a model was trained using a particular dataset; when in reality, it was trained on another. In effect, these attacks *forge* one dataset into another *distinct* dataset that produces the same model. Given the true training set  $D$ , a forgery  $D'$  may be produced along with sufficient proof claiming that  $D'$  is the real training set, not  $D$ . Thus, data forging attacks appear to throw into jeopardy the question of ever determining exactly what data a model was trained on.

**Data Forging.** At a high level, given a machine learning model’s true training dataset  $D$ , a data forging attack produces

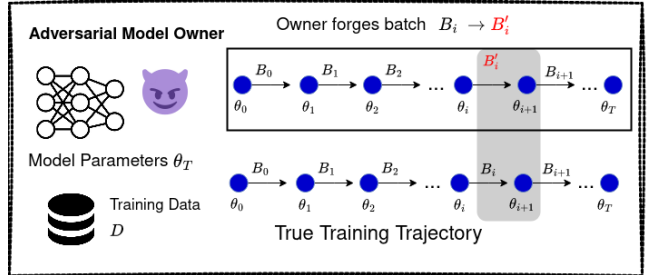


Fig. 1: The adversarial model owner has access to the true execution trace denoting the sequence of model parameters and associated mini-batches. When performing a data forging attack, the model owner *forges* (i.e., replaces) a batch  $B_i$  such that  $(x, y) \in B_i$  with a different batch  $B'_i$  not containing  $(x, y)$  such that the resulting models are nearly identical.

a claim that the model is the result of training on a *different* dataset  $D'$ , by forging  $D$  into  $D'$ . To achieve this, data forging attacks rely on the fact that supervised training uses iterative algorithms such as Stochastic Gradient Descent (SGD). These algorithms produce a sequence consisting of model parameters (or *checkpoints*) and associated mini-batches, starting with the random initialisation and ending with the final trained model parameters. Such a sequence, or *execution trace*, may be *verified* by a third party, who reproduces each checkpoint in the sequence, using the mini-batch and parameters from the previous checkpoint, and ensures that what they have recomputed and the current checkpoint are nearly identical, i.e., the  $\ell_2$  distance between the two sets of model parameters is below a given *small* non-zero error threshold  $\epsilon$ . A non zero threshold may be allowed due to noise that stems from hardware and software factors. Specifically, there are small numerical deviations between repeated recomputations of any particular checkpoint due to benign noise (see Section II-B for a detailed discussion on the source of these errors). A data forging attack replaces one or more mini-batches in the execution trace with *forged* (i.e., different) mini-batches that produce nearly (i.e., within reproduction error) identical gradient updates, and falsely claims that the model checkpoints present in the execution trace are actually the result of training on these forged mini-batches, not the original mini-batches that were replaced.

**Privacy Implications.** Existing works [23], [12], [29] have noted that data forging has clear implications for two large concepts within machine learning and privacy; namely (i)

membership inference, and (ii) machine unlearning. Membership inference attacks (MIAs) [20], [6], [10] have been developed in order to determine whether a particular data record was part of the model’s training dataset. Suppose that the training example  $(\mathbf{x}, \mathbf{y})$  is indeed a member of the model’s training set; an adversary may refute this claim by forging the true dataset  $D$  into another  $D'$  such that  $(\mathbf{x}, \mathbf{y}) \notin D'$  (see Fig. 1), calling into question the veracity of membership inference attacks. Performing such an attack is also equivalent to claiming that  $(\mathbf{x}, \mathbf{y})$  has been “unlearnt”, as by the definition of *exact unlearning* [4], the final model parameters are the result of training on a dataset that does not contain  $(\mathbf{x}, \mathbf{y})$ . Importantly, the adversary does not have to perform any actual re-training, resulting in two equally valid claims that appear to contradict each other; the model has been both trained and not trained using  $(\mathbf{x}, \mathbf{y})$ . Machine unlearning [26], [4], [5] has emerged as a response to GDPR’s [25] *right to be forgotten* framework, and prior work [23], [29] note how data forging can undermine the concept, and in its wake, call for the research and development of auditable machine unlearning.

The seriousness of these implications hinges on the performance of the data forging attacks, i.e., *how identical are the gradients between original and forged mini-batches produced by these attacks?* This metric, known as approximation error, is given by the  $\ell_2$  norm between the forged model update and the original present in the execution trace.

Within the data forging literature, there exists a dichotomy of assumptions on how small this approximation error should be in order to fully realise the implications discussed previously. Prior data forging works [12], [23], [29] argue that their attacks produce approximation errors that are indistinguishable from benign reproduction errors. On the other hand, Baluta et al. [3] argue against the acceptance of any error, citing that floating point operations are deterministic and there should be zero error when recomputing execution traces. Baluta et al. [3] go on to prove that zero error, or *exact* data forging is not possible using existing attack methods. As a result, they find that existing data forging attacks do not pose any risk to membership inference or machine unlearning as they are easily detectable by the presence of non zero error.

While the  $\epsilon = 0$  scenario posed by Baluta et al. [3] is possible if the original hardware and software are available during verification (and may be necessary in certain high stakes scenarios such as medical data), it is unrealistic to always impose such a strict setting in practice. Particularly when the original hardware and software is not available, it is not practical, and often impossible, to avoid benign hardware reproduction errors. We argue that data forging attacks fully realise their implications only if their approximation errors are of the same order of magnitude as these benign reproduction errors. Prior data forging works [12], [23], [29] do not justify the level of approximation error generated by their attacks, and largely ignore this pertinent question regarding their performance.

**Contributions.** We list our contributions to data forging as the following:

- 1) We provide the first thorough evaluation of the magnitude of reproduction errors across several hardware platforms and for several model architectures.
- 2) We find that the approximation errors produced by existing data forging attacks are too large, often several orders of magnitude larger than observed reproduction errors. This makes existing attacks easily detectable, nullifying their privacy impact in practice.
- 3) The current theoretical analysis of data forging in Baluta et al. [3] is restricted to the existing instantiations of data forging attacks and necessitates the investigation of broader potential attack strategies. To tackle this, we extend their analysis, addressing more general questions regarding the existence of distinct mini-batches that produce the same gradient and how they may be constructed. Focusing on fully connected neural networks, we formulate the problem of exact data forging as a system of linear equations, where each solution corresponds to a forged mini-batch. Of the infinite solutions that may exist, finding those that correspond to a distinct, valid mini-batch i.e., one that falls within the domain of allowed training examples (e.g., in the case of images, pixel values between 0 – 255 and one hot labels) is a non-trivial task, and one that we conjecture may be computationally infeasible, even for relatively simple linear models such as logistic regression.

As a result, we call for a re-evaluation of existing attacks, and for further research into this nascent attack vector against machine learning.

## II. BACKGROUND

### A. Execution Traces

Supervised machine learning is a process to learn a *model*, in particular, a parameterized function  $f_\theta : \mathcal{X} \rightarrow \mathcal{Y}$ . The parameters are typically optimized by applying iterative methods such as Stochastic Gradient Descent (SGD) to a training set. At the  $i$ -th gradient descent step, the next set of model parameters  $\theta_{i+1}$  is calculated from the previous set of parameters  $\theta_i$  and a mini-batch  $B_i$  sampled from the dataset  $D = \{(\mathbf{x}^{(i)}, \mathbf{y}^{(i)})\}_{i=1}^N$ . Starting with a random initialisation  $\theta_0$ , the final model  $\theta_T$  is the result of performing  $T$  total gradient descent steps iteratively. This results in a sequence of intermediate model parameters  $\theta_0, \theta_1, \theta_2, \dots, \theta_T$ , and sampled mini-batches  $B_0, B_1, B_2, \dots, B_{T-1}$  that trace out a *training trajectory*. A  $k$ -intervaled *execution trace* consists of a set of model checkpoints after every  $k$  steps

$$\theta_0, \theta_k, \theta_{2k}, \dots, \theta_{ik}, \dots, \theta_{\frac{T}{k} \cdot k},$$

and sequences of one or more mini-batches

$$\left\{ \{B_j\}_{j=ik}^{(i+1)k-1}, : i \in \{0, 1, 2, \dots, \frac{T}{k} - 1\} \right\}.$$

Each  $\theta_{(i+1)k}$  is produced by training  $\theta_{ik}$  on the sequence of mini-batches  $\{B_j\}_{j=ik}^{(i+1)k-1}$  using gradient descent:

$$\theta_{(i+1)k} := \theta_{ik} - \sum_{j=ik}^{(i+1)k-1} \eta \nabla_{\theta} \mathcal{L}(B_j; \theta_j).$$

The execution trace  $S$  is then given by the set of tuples of the form

$$S := \{(\theta_{ik}, \{B_j\}_{j=ik}^{(i+1)k-1})\}_{i=1}^{(T/k)-1} \cup \{(\theta_T, \emptyset)\},$$

capturing the training trajectory of the model. When  $k = 1$ , the execution trace is simply  $S := \{(\theta_0, B_0), (\theta_1, B_1), (\theta_2, B_2), \dots, (\theta_{T-1}, B_{T-1}), (\theta_T, \emptyset)\}$

### B. Reproduction Errors

Recent work by Schlögl et al. [19] found that runtime optimisations of machine learning frameworks can result in non-deterministic numerical deviations in the outputs of neural networks. Schlögl et al. cite auto-tuning [9] as the root cause. This is a process whereby microbenchmarks executed just before inference determine what optimisations to apply to the given operation e.g., the results of the microbenchmarks determine which GPU kernel gives the best performance on a given hardware and input shape. A well known property of floating point arithmetic is that addition is not associative, that is, it is not necessarily the case that  $(a+b)+c = a+(b+c)$ , but may be off by a small error. These auto-tuning optimisations can lead to changes in the aggregation order of intermediate results from kernel to kernel, resulting in deviations in the final output of a neural network, even for the same input. In the context of execution traces for machine learning models, this means that given the same random initialisation  $\theta_0$  and the same sequence of mini-batches  $B_0, B_1, B_2, \dots, B_{T-1}$ , the resulting checkpoints  $\theta_1, \theta_2, \theta_3, \dots, \theta_T$  will differ between repeated recomputations due to auto-tuning.

### C. Data Forging

Thudi et al.'s [23] concepts of *forgeability* and data forging attempt to produce distinct execution traces for a given model  $\theta_T$  using the same checkpoints, but with different e.g., *forged* mini-batches. At a high level, Thudi et al. claim that any mini-batch from an execution traces may be *forged* (i.e., replaced) with another containing different training data, yet still produce a nearly identical gradient descent update. *Data forging attacks* against execution traces attempt to construct, for a given mini-batch  $B_i$ , a forged (i.e., distinct) counterpart  $B'_i$  such that the next model in the execution trace, when calculated using  $B'_i$  is *nearly* identical to  $\theta_{i+1}$  i.e., the approximation error  $\|(\theta_{i+1} - (\theta_i - \eta \nabla_{\theta} \mathcal{L}(B'_i; \theta_i)))\|_2$  is minimal. The attacks proposed in [23], [12] construct forged mini-batches by randomly sampling *other* training examples from the dataset. These attacks were introduced in the context of *deleting* a set  $U \subset D$  of training examples from an execution trace, and work by *greedily searching* over the set of training examples  $D \setminus U$ . A *greedy search* attack works in three steps:

- 1) Sample  $n$  data points uniformly from  $D \setminus U$ .

- 2) Sample  $M$  mini-batches  $\{\hat{B}_1, \dots, \hat{B}_M\}$  uniformly from the selected  $n$  data points.
- 3) Out of the  $M$  mini-batches  $\{\hat{B}_1, \dots, \hat{B}_M\}$ , select the mini-batch  $\hat{B}_j$  that minimises  $\|\theta_{i+1} - (\theta_i - \eta \nabla_{\theta} \mathcal{L}(\hat{B}_j; \theta_i))\|_2$ , and output the forged mini-batch  $B'_i = \hat{B}_j$ .

Thudi et al. introduced this type of forging approach, and Kong et al. improve upon its efficiency, with similar performance. Recently, Zhang et al. [29] augmented this approach by choosing to instead replace data points  $(\mathbf{x}, \mathbf{y}) \in U$  with their class-wise nearest neighbour from  $D \setminus U$ .

### III. DATA FORGING THREAT MODEL

In Algorithm 1, we formulate a general data forging game between an adversary  $\mathcal{A}$  and a verifier  $\mathcal{V}$ . Our formulation generalises the data forging game in [3], and captures the setup proposed in previous data forging works [12], [23], [3], [29]. We allow for a non zero error between recomputed and original checkpoints in contrast to [3], who required  $\epsilon = 0$ . Section V discusses in greater detail why such a generalisation is necessary in practice.

---

**Algorithm 1** The data forgery game between  $\mathcal{A}$  and  $\mathcal{V}$ .

**Input:** Adversary  $\mathcal{A}$ , Verifier  $\mathcal{V}$ , Training algorithm  $\mathcal{T}$ , Dataset  $D$ , error threshold  $\epsilon$ , checkpointing interval  $k$ , batch size  $b$

**Output:** ACCEPT or REJECT

- 1:  $\mathcal{V}$  produces execution trace  $S \leftarrow \mathcal{T}(D, b, k)$ .
- 2:  $\mathcal{V}$  chooses a random index  $t \in \{0, 1, 2, 3, \dots, T-1\}$ .
- 3: Adversary forges mini-batch  $B_t$  into  $B'_t \leftarrow \mathcal{A}(S, D, t)$ .
- 4: **if**  $(B'_t = B_t)$  or  $(\exists (\mathbf{x}', \mathbf{y}') \in B'_t \text{ s.t. } (\mathbf{x}', \mathbf{y}') \notin \mathcal{X} \times \mathcal{Y})$  **then**
- 5:     **return** REJECT
- 6: **end if**
- 7:  $\mathcal{V}$  chooses  $i$  such that  $ik \leq t < (i+1)k$
- 8:  $\mathcal{V}$  calculates  $\theta_{(i+1)k}^{\mathcal{V}} \leftarrow \theta_{ik} - \eta \sum_{j=ik}^{(i+1)k-1} \nabla_{\theta} \mathcal{L}(B_j; \theta_j)$  on their own hardware using  $B'_t$  when  $j = t$ .
- 9:  $\mathcal{V}$  calculates the error  $\epsilon_{(i+1)k} \leftarrow \|\theta_{(i+1)k} - \theta_{(i+1)k}^{\mathcal{V}}\|_2$
- 10: **if**  $(\epsilon_{(i+1)k} > \epsilon)$  **then**
- 11:     **return** REJECT
- 12: **else**
- 13:     **return** ACCEPT
- 14: **end if**

---

The game plays as follows: the verifier begins by first running the training algorithm  $\mathcal{T}$  e.g., stochastic gradient descent on dataset  $D$  for  $T$  steps, and produces execution trace  $S$ , saving every  $k$ -th checkpoint. The verifier then challenges the adversary to forge a random batch  $B_t$  from  $S$ . The adversary has access to the full execution trace and the dataset, and is capable of instantiating any data forging attack algorithm in order to produce the corresponding forged mini-batch  $B'_t$ , which must satisfy the following initial conditions:

- $B'_t \neq B_t$ . Adversaries participating in the game must produce a forged mini-batch that is *different* from the original in at least one example.

- $(\mathbf{x}', \mathbf{y}') \in \mathcal{X} \times \mathcal{Y}, \quad \forall (\mathbf{x}', \mathbf{y}') \in B'_t$ . This condition constrains each forged training example  $(\mathbf{x}', \mathbf{y}')$  to be within the domain of the training context *e.g.* pixel values between 0 – 255 and one hot labels.

Finally, the verifier reproduces the appropriate checkpoint  $\theta_{(i+1)k}$  such that the batch  $B_t$  lies in the set of batches used to obtain  $\theta_{(i+1)k}$ , *i.e.*, choose  $i$  such that  $ik \leq t < (i+1)k$ . The verifier computes  $\theta_{(i+1)k}^{\mathcal{Y}}$  using the forged mini-batch  $B'_t$  produced by the adversary instead of  $B_t$ . Then, the adversary calculates the  $\ell_2$  error  $\epsilon_{(i+1)k} := \|\theta_{(i+1)k} - \theta_{(i+1)k}^{\mathcal{Y}}\|_2$  between their recomputed checkpoint, and the one present in the trace. The game ends with a REJECT result if  $\epsilon_{(i+1)k} > \epsilon$ , otherwise the game ends with ACCEPT *i.e.*, the adversary wins. The reproduction error threshold  $\epsilon$  is a parameter of the game that defines how large the  $\ell_2$  between a recomputed model and the original model may be. We introduce the notion of **stealthy data forging** which refers to the production of a forged mini-batch  $B'_t$  that wins the above data forging game. Concretely, this means that attacks that produce a  $B'_t$  whose approximation error is less than or equal to the chosen threshold  $\epsilon$  are deemed *stealthy*.

#### IV. ARE CURRENT DATA FORGING ATTACKS STEALTHY?

Previous data forging works [12], [23], [29] have employed data forging as a means of adversarially *deleting* data from a model’s execution trace *i.e.*, for a given set of training examples  $U \subset D$ , these attacks forge the true dataset  $D$  into another  $D'$  such that  $D' \cap U = \emptyset$ . Kong et al. [12] note that if you can delete training examples from an execution trace by replacing them with forged examples, you can provably refute a membership inference claim against them. Additionally, [23], [29] observe that if you perform the same replacement, you can also claim to have “unlearnt” those training examples.

These implications of data forging are only fully realised if the attacks are *stealthy* *i.e.*, the win the game with an approximation error lower than the error threshold chosen by the verifier. A verifier will choose their error threshold  $\epsilon$  to be no larger than observed reproduction errors. As a result, for a data forging attack to be stealthy, its approximation errors must be on the same order of magnitude as reproduction errors. Stealthiness derives from the fact that the approximation errors would be indistinguishable from the regular noise that pervades floating point computation.

In order to answer the question of whether existing attacks are stealthy, we first conduct experiments to determine the magnitude of reproduction errors, and compare this to the approximation errors produced by existing attacks. In the next section, we perform repeated recomputations of execution traces<sup>1</sup>, and measure the  $\ell_2$  distance between repeated recomputations, in order to characterise the magnitude of reproduction errors. Subsequently, we compare the magnitude of our observed hardware errors to the magnitude of the approximation errors produced by the data forging attacks developed in [12], [23], [29]. **Our findings suggest that existing**

<sup>1</sup>Existing works [12], [3], [23], [29] consider the  $k = 1$  scenario, and we do so here as well in order to evaluate them.

**data forging attacks are not stealthy** *i.e.*, reproduction errors are often orders of magnitude smaller than approximation errors produced by existing data forging attacks.

#### A. What is the Magnitude of Benign Reproduction Errors?

In order to quantify their magnitude, we perform experiments where a model is trained on a dataset for  $T$  total steps, producing a  $k = 1$  intervalled execution trace. We then recompute this trace, on the same and different hardware, and measure the distance between every recomputed checkpoint and the corresponding original checkpoint. The magnitude of the error between repeated recomputations of the same checkpoint is called the *reproduction error*, and is calculated using the  $\ell_2$  norm  $\epsilon_{repr} := \arg \max_i \epsilon_{(i+1)}$  *i.e.*, the reproduction error is the largest observed  $\ell_2$  distance between recomputations.

**Experimental Details:** We produce  $k = 1$  intervalled execution traces for LeNet [1] (61.7K parameters) trained on MNIST [14] and VGGmini [22] (5.75M parameters) trained on CIFAR10 [13]. We keep the learning rate fixed at  $\eta = 0.01$ . For all our experiments, we use TensorFlow v2.15.0, CUDA v12.2, and CUDNN v8.9. We use the same models, datasets, checkpointing interval, and learning rate as used by previous data forging works [12], [23], [29]. For a given execution trace (*e.g.*, a trace produced for a given model, dataset, batch size  $b$ , and on a given hardware & software platform), our experiments proceed as follows:

- 1) First, we choose the hardware platform where the execution trace will be recomputed *i.e.*, this is either the same GPU it was generated on or a different one.
- 2) We recompute each checkpoint by loading  $\theta_i$  from the execution trace and training on the corresponding mini-batch  $B_i$ , also taken from the execution trace.
- 3) We measure the distance between our recomputed checkpoint and the corresponding checkpoint  $\theta_{i+1}$  present in the execution trace.
- 4) We repeat this process multiple times and report the largest observed distance for each recomputed checkpoint.

The question of what might affect the magnitude of reproduction errors boils down to the question of what might affect the results of the auto-tuning microbenchmarks that ultimately decide which floating point operations are done in which order. It is possible (however unlikely), that two training runs, starting with the same random initialisation and using the same sequence of mini-batches, may produce the exact same sequence of checkpoints (*i.e.*, zero reproduction error) simply by chance. In reality, reproduction errors occur because the likelihood that the floating point operations are done in the same order after auto-tuning between two different training runs is very small. What goes into the decision of gpu kernel can depend on a host of reasons such as the model architecture, dataset, the particular hardware and software, the other processes that are running on the machine at the time, etc. A comprehensive analysis of all these factors is beyond the scope of this work. However, keeping the software fixed

and ensuring that no other processes are running on the GPU, we attempt to answer the following questions regarding the magnitude of reproduction errors:

- 1) *How large are the reproduction errors when recomputing execution traces using the same hardware that generated them?*
- 2) *How large are the reproduction errors when recomputing execution traces on a different hardware from the one that generated them?*

1) **Recomputation on the same hardware:** Table I reports the largest observed reproduction error for our two setups on the same hardware for  $k = 1$  intervalled execution traces *i.e.*, every model update is saved as part of the trace. We train LeNet for  $T = 1200$  steps with varying batch sizes and VGGmini for  $T = 2500$  steps. We produced the execution traces on a NVIDIA GeForce RTX 4090 GPU with **auto-tuning turned on, finding that reproduction errors were consistently on the order of magnitude of  $10^{-8}$ , when recomputing execution traces on the same GPU that generated them.** Neither batch size nor model size appeared to affect the magnitude of these errors, and we found little deviation between consecutive recomputations *i.e.*, the errors were always within the same order of magnitude over several recomputation runs. No other processes were running<sup>2</sup> on the RTX 4090 GPU during both the initial generation and recomputation of the execution traces.

TABLE I: The largest observed reproduction error when recomputing execution traces on the same hardware that generated them. For this table, we generated execution traces on a RTX 4090 and recomputed them on the same GPU. During the generation and recomputation, auto-tuning was turned on.

Model/Dataset (batch size)	Largest observed $\epsilon_{repr}$
LeNet/MNIST (100)	$10^{-8}$
LeNet/MNIST (500)	$10^{-8}$
LeNet/MNIST (1000)	$10^{-8}$
VGGmini/CIFAR10 (100)	$10^{-8}$
VGGmini/CIFAR10 (500)	$10^{-8}$
VGGmini/CIFAR10 (1000)	$10^{-7}$

2) **Recomputation on different hardware:** We now attempt to characterise the magnitude of benign hardware errors when the recomputation is done on a different GPU than the one that produced the execution trace. In Table II, we report the largest observed reproduction error for cross hardware recomputation. We consider two different GPUs in our experiments: a RTX 4090 and a Tesla V100. We find that **recomputing execution traces on different hardware can produce slightly larger levels of error** compared to when recomputation is done on the original hardware. In our cross-hardware experimentation, we found that the error increases only by a single order of magnitude. On both GPUs, auto-tuning is turned on.

In most machine learning applications, auto-tuning is turned on as it boosts performance, however, widely used machine

	RTX 4090	Tesla V100
RTX 4090	$10^{-8}$	$10^{-7}$
Tesla V100	$10^{-7}$	$10^{-8}$

(a) LeNet/MNIST  $b = 100$

	RTX 4090	Tesla V100
RTX 4090	0	$10^{-6}$
Tesla V100	$10^{-6}$	0

(b) Deterministic LeNet/MNIST  $b = 100$

	RTX 4090	Tesla V100
RTX 4090	$10^{-8}$	$10^{-7}$
Tesla V100	$10^{-7}$	$10^{-8}$

(c) LeNet/MNIST  $b = 1000$

TABLE II: The largest observed  $\epsilon_{repr}$  for  $k = 1$  interlaved traces when recomputation is done on different hardware. For a given execution trace setup (*i.e.*, each subtable), each row indicates the GPU the execution trace was generated on and the column indicates which GPU the trace was recomputed on. In Tab. IIb, the diagonal entries are zero because deterministic training results in zero error when recomputing on the same hardware.

learning frameworks such as TensorFlow [2] and PyTorch [18] provide an option to turn it off<sup>3</sup>. We found that turning auto-tuning off results in zero error when recomputing execution traces using the same hardware and software, as the floating point operations occur in a deterministic order that is set by an initial seed. However, different hardware platforms may not share the same implementations of algorithms *i.e.*, they may differ in approach and aggregation order, **resulting in unavoidable reproduction error, even if auto-tuning is turned off**. Table IIb shows how when auto-tuning is off e.g., in deterministic training, there is zero error when the execution trace is generated and recomputed on the same hardware. However, when the generating and recomputing hardware differ, we found that the reproduction error is non zero, and during our experiments, was larger than when auto-tuning is turned on. **In all our experiments, the largest reproduction errors we observed were on the order of  $10^{-6}$ , which occurred only during cross-hardware recomputation. When recomputing checkpoints on the same hardware, the largest errors we observed were on the order of  $10^{-7}$ .**

### B. Evaluating the Performance of Existing Data Forging Attacks: How Small are their Approximation Errors?

In this section, we perform data forging attacks against the execution traces we generated in the previous section, and report their approximation error. Our results highlight two important factors that affect the approximation error; namely the forging fraction (*i.e.*, the number of examples in a mini-batch that need to be replaced), and the stage of training at which forging is taking place.

<sup>2</sup>Except the desktop environment. We conjecture that the auto-tuning microbenchmarks are affected by what else is running on the GPU, however we do not conduct extensive experiments to this end.

<sup>3</sup>See [https://www.tensorflow.org/api\\_docs/python/tf/config/experimental/enable\\_op\\_determinism](https://www.tensorflow.org/api_docs/python/tf/config/experimental/enable_op_determinism) and <https://pytorch.org/docs/stable/notes/randomness.html>

1) **Smaller forging fractions result in smaller approximation errors:** Recall that the goal of the adversary is to replace the original mini-batch  $B_i$  with a forged mini-batch  $B'_i$  such that  $U \cap B'_i = \emptyset$ . The difficulty of producing the forged mini-batch  $B'_i$  is proportional to the cardinality of  $B_i \cap U$ . If  $\#(B_i \cap U) = 1$ , *i.e.*, only one example needs to be forged, then the adversary can keep all the other  $b - 1$  examples the same in  $B'_i$  and only forge the single training example. For larger values of  $b$ , the effect of a single example on the average gradient  $\nabla_{\theta} \mathcal{L}(B'_i)$  becomes negligible; regardless of what the training example is replaced with, its effect on the average gradient is essentially “drowned out” by the other  $b - 1$  training examples that are shared between  $B_i$  and  $B'_i$ . Given a fixed number of training examples in  $B_i$  that needs to be replaced, for larger and larger batch sizes (*i.e.*, *smaller forging fractions*  $\frac{\#(B_i \cap U)}{\#(B_i)}$ ), we expect the approximation error to get smaller. However, if  $\#(B_i \cap U) = \#(B_i) = b$ , then forging is much more difficult, as every example needs to be replaced. Figure 2 shows that this expected behaviour is indeed observed when forging both LeNet/MNIST and VGGmini/CIFAR10 traces. We see that the attacks perform best (*i.e.*, produce the smallest approximation errors) when the forging fraction  $\frac{\#(B_i \cap U)}{\#(B_i)} = \frac{1}{b}$ , and degrade quickly with increased forging fractions. We also observe that Thudi et al. [23] and Zhang et al. [29]’s attacks have similar performance (see Appendix C for a comparison).

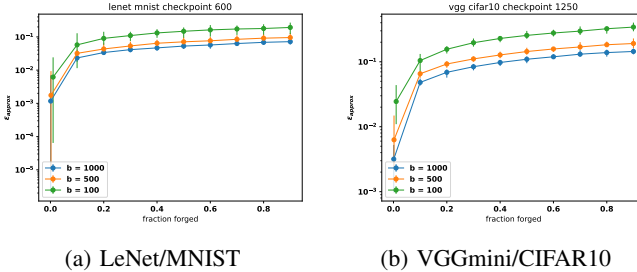


Fig. 2: The average approximation error of Thudi et al.’s attack [23] (over several runs), as well as the min and max observed approximation error for different batch sizes and increasing forging fractions. Performance degrades quickly with increased forging fraction. In both settings, we forge the middle checkpoint of the execution trace.

## 2) Forging performance is inconsistent across training:

In addition to forging fraction, we postulate that the stage of training at which forging is being performed may affect the performance of these attacks. We run the following experiment to evaluate this:

- 1) For a given execution trace’s training trajectory  $\theta_0, \theta_1, \dots, \theta_T$ , we sample a true mini-batch  $B$  and calculate its model update at different checkpoints across the execution trace *i.e.*, we calculate  $\theta_i - \eta \nabla_{\theta} \mathcal{L}(B; \theta_i)$  for values of  $i$  across training.
- 2) We then forge mini-batch  $B$  into  $B'$  across training at each checkpoint and measure the approximation error.
- 3) We repeat this several times for different sampled mini-batches in order to study the variance.

In Figure 3, we plot the approximation error produced by Thudi et al.’s forging attack over several runs (*i.e.*, different true mini-batches) across checkpoints from LeNet/MNIST and VGGmini/CIFAR10 execution traces (batch size of 1000). In Figure 3a, when the forging fraction is  $\frac{1}{1000}$  we see that Thudi et al.’s attack is inconsistent across the checkpoints of a LeNet/MNIST execution trace. For a given batch, the forgery produced may have an approximation error that ranges from  $10^{-7}$  all the way up to  $10^{-2}$ . For some mini-batches, the approximation error increases with training, for others, it decreases. However, when the forging fraction is 1, the attack’s performance is best early in training, producing approximation errors near  $10^{-2}$ , which then rises to near  $10^{-1}$  and remains there for the rest of training. In Figures 3c and 3d, we see similar behaviour for VGGmini/CIFAR10 traces; when the forging fraction is  $\frac{1}{1000}$ , we observe large variations in approximation errors (from  $10^{-4}$  to nearly  $10^{-2}$ , and conversely, much more consistent performance that spans only a single order of magnitude when the forging fraction is 1.

## C. Is Data Forging Stealthy?

From our experimentation in Section IV-A, we found that benign reproduction error was typically around  $10^{-8}$ , and could reach as large as  $10^{-6}$ , when the recomputation was done on different hardware. Therefore, in order for data forging attacks to be considered stealthy, they must produce approximation errors on the order of at least  $10^{-6}$  or smaller. **From our evaluation of the existing data forging attacks, they cannot be classed as stealthy.** While factors such as forging fraction and the stage of training affect the performance of these attacks, overall they are not stealthy. In particular, we found existing attacks could produce stealthy levels of approximation error only in one scenario: when forging a LeNet/MNIST execution trace late in training with a forging fraction of  $\frac{1}{1000}$ . Even in this narrow case, when the forged and true mini-batches share 999 examples, existing attacks could not reliably forge with sufficiently small reproduction errors (see variance in Figure 3a). Even if the set of examples that need to be deleted  $U = \{(\mathbf{x}, \mathbf{y})\}$  *i.e.*, it consists of just a single example, existing attacks cannot stealthily forge, as this training example would occur in mini-batches early in training (LeNet/MNIST ( $b = 1000$ ) execution traces capture 20 epochs of training), and data forging early in training is not stealthy *i.e.*, approximation errors early in training are nearly 5 orders of magnitude larger than reproduction errors.

For more complex models and datasets like VGGmini/CIFAR10, the attacks were never stealthy, even under small forging fractions of  $\frac{1}{1000}$  they produce approximation errors of  $10^{-3}$  (see Figure 2b), 5 orders of magnitude larger than benign reproduction errors, which are around  $10^{-8}$ . This points to the over-reliance of these *greedy-search* style forging attacks on the existence of other, similar data that may be used. Datasets like MNIST do not vary much; for a given image of a digit, there is likely another, very similar one, however this is not the case for CIFAR10, which may explain the poor performance of existing data forging attacks. Table III summarises our

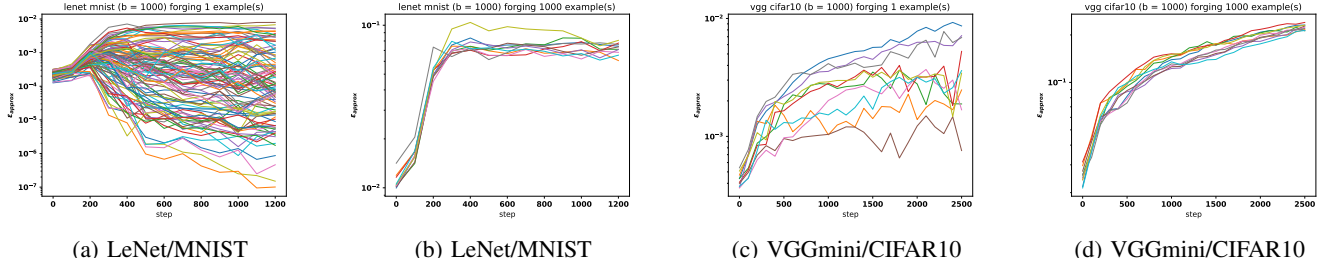


Fig. 3: Approximation errors produced by Thudi et al.’s attack [23] across the stages of training. Each line corresponds to a different true mini-batch  $B$ , and the y-axis reports the approximation error when trying to forge  $B$  at the given step on the x-axis. We see that the performance is inconsistent when the forging fraction is  $\frac{1}{b}$  (see Figures 3a and 3c). When the forging fraction is 1 (see Figures 3b and 3d), approximation errors are consistent across different batches and increase with training.

evaluations, showing in exactly which situations current data forging approaches were able to produce stealthy forgeries.

	$\frac{\#(B \cap U)}{\#(B)} = \frac{1}{b}$	$\frac{\#(B \cap U)}{\#(B)} = 1$
Early Training	$10^{-4}$ (X)	$10^{-2}$ (X)
Late Training	$10^{-7}$ (!)	$10^{-1}$ (X)

(a) LeNet/MNIST

	$\frac{\#(B \cap U)}{\#(B)} = \frac{1}{b}$	$\frac{\#(B \cap U)}{\#(B)} = 1$
Early Training	$10^{-4}$ (X)	$10^{-2}$ (X)
Late Training	$10^{-4}$ (X)	$10^{-1}$ (X)

(b) VGGmini/CIFAR10

TABLE III: We show the smallest approximation error produced under different cases for LeNet/MNIST and VGGmini/CIFAR10 execution traces. A X is given in those situations where existing attacks were never stealthy. A ! is given only in the case of small forging fractions and at the later stages of training for LeNet/MNIST of  $b = 1000$  traces only. Even in this case, the performance of the attacks was found to be inconsistent (see Figure 3a).

## V. CHOOSING AN ERROR THRESHOLD IN PRACTICE IS HARD

From our experimentation, we have seen that existing attacks are not stealthy when the error threshold  $\epsilon$  is chosen to be no larger than benign reproduction errors. However, determining this value accurately can be tricky when it is not possible to perform cross hardware recomputation. Consider the following scenario that highlights the difficulty of correctly setting  $\epsilon$  in practice: a verifier intends to verify a LeNet/MNIST ( $b = 100$ ) execution trace on a RTX4090 GPU. They set  $\epsilon = 10^{-8}$  for their error threshold as this is their observed level of reproduction error on their hardware<sup>4</sup>. Now suppose that the model owner is honest and trained their model using a Tesla V100 GPU. From our experimentation, we found that the reproduction error of honest traces generated using a V100 and recomputed on a RTX4080 can be as large as  $10^{-6}$  (See Table IIb). As a result, even the honest trace would not pass verification if  $\epsilon = 10^{-8}$ . One of the

<sup>4</sup>See the corresponding row in Table I for LeNet/MNIST ( $b = 100$ ).

challenges of building robust verification schemes is that, as we have seen, reproduction errors can vary by several orders of magnitude depending on the hardware that the checkpoints were generated on, as well as the hardware they are reproduced on.

Within the data forging literature, there is a difference of opinion on what is an acceptable choice of  $\epsilon$ . Baluta et al. [3] consider only the scenario of a strict verifier that always selects  $\epsilon = 0$ . They assert that given (i) the initial random seed(s) used during training, (ii) the original software, and (iii) the original hardware the computations were performed on, there should be zero error between recomputations of any given execution trace. They claim that since the entire computation sequence is deterministic, error at any step of reproduction of the execution trace must therefore point to foul play. While it is true that reproduction error can be eliminated given these conditions<sup>5</sup> and may be necessary in high stakes applications such as medical machine learning models, we argue that always demanding  $\epsilon = 0$  is unrealistic in practice, particularly when the original hardware is not available.

Due to the existence of reproduction error, prior data forging works [12], [23], [29] have recognised the practical necessity of a non-zero threshold during verification, and consider the  $\epsilon > 0$  scenario. While their attacks produce non-zero approximation errors, the question of whether a verifier should accept the levels of approximation error generated by their attack algorithms is largely overlooked by the prior work. They provide no analysis of how large reproduction errors can be and whether their attack algorithms produce approximation errors that are comparable. In this work, we have conclusively determined that this is not the case; reproduction errors are orders of magnitude smaller than the approximation errors produced by existing attacks.

Verifiers are therefore met with a tradeoff when choosing their error threshold. Seeking to not reject honest traces, and being cognisant of the fact that there may exist other factors that affect reproduction errors; they set their threshold to be larger than the reproduction errors which they have observed

<sup>5</sup>See Table IIb, where we observed zero reproduction error when the original random seeds, hardware, and software were used for the recomputation.

through experimentation. However, in doing so, they allow for data forging attacks, that would have not been stealthy under a stricter choice of error threshold, to become stealthy, thus exploiting the verifier’s pragmatism. A similar situation is seen in the area of Differential Privacy (DP) [7]. A privacy parameter  $\epsilon$  is chosen to determine how private<sup>6</sup> a given function is. Within DP, ideally  $\epsilon < 1$ , however, choosing such a small epsilon can hinder the performance of the model. We have a similar setup here, where  $\epsilon = 0$  gives the verifier the most confidence in their reproductions, however this may not be practical all the time, necessitating the choice of larger error thresholds. Large error thresholds  $\epsilon$ , larger batch sizes  $b$ , and smaller forging fractions allow for more *wiggle room*, increasing the likelihood of potential foul play from data forging. Certain heuristics may be developed for the choice of error threshold *e.g.*, set  $\epsilon$  no larger than 2 orders larger than observed reproduction errors, however further research into more robust schemes is necessary. We leave this for future work.

## VI. ON THE DIFFICULTY OF EXACT DATA FORGING

Existing data forging attacks attempt to find, for a given mini-batch  $B$ , a distinct counterpart  $B'$  such that their gradients are *approximately* the same. In previous sections, we have examined how similar the gradients of the original and forged mini-batches produced by existing “greedy search” style attacks [12], [23], [29] are, and found that the magnitude of their approximation errors are too large, allowing us to classify existing data forging attacks as not stealthy. However, little work has been devoted to *exact* data forging *i.e.*, developing data forging attacks that produce forged mini-batches with the *same* gradient. The related subject of gradient inversion [33], [17], [28], [31], [27], [32] asks the reverse question: *given the gradient  $\nabla_\theta \mathcal{L}(B)$ , can the original mini-batch  $B$  be recovered?* This question is pertinent to the area of Federated Learning [16], as the gradients of sensitive information are sent among several parties; and an analysis of the privacy impact of sharing these gradients is required. Within data forging, we are concerned with a related question: *given mini-batch  $B$  and its gradient  $\nabla_\theta \mathcal{L}(B)$ , does there exist another, distinct, mini-batch  $B'$  such that  $\nabla_\theta \mathcal{L}(B) = \nabla_\theta \mathcal{L}(B')$ ?* Any error when reproducing the gradients of such a  $B$  and  $B'$  can only ever be at most, as large as reproduction error, resulting in stealthy data forging. Consequently, this question is of great importance to an adversarial model owner looking to perform stealthy data forging.

A key limitation of prior data forging attacks is the usage of the finite search space  $D \setminus U$  when searching for replacements. Baluta et al. [3] analysed the models and datasets considered by the prior work. They find that the execution traces considered by the prior work are *unforgeable* using existing

<sup>6</sup>Privacy in DP is quantified by how much the output of a function differs for inputs that differ by one datapoint. If they do not differ by much, then inferring whether a datapoint was or was not part of the input is difficult. This difficulty of inference is inversely proportional to the privacy parameter  $\epsilon$ .

techniques *i.e.*, these attacks cannot produce a forged mini-batch with, analytically, the same gradient. However, there may exist training examples outside  $D \setminus U$  that result in zero error. This section is devoted to answering the question of exact data forging *i.e.*, the search for mini-batches outside  $D \setminus U$  that result in zero error. Our analysis suggests that while it is possible to construct a distinct mini-batch  $B'$  that produces the same gradient, analytically, as  $B$ , finding a  $B'$  within the allowed input space  $\mathcal{X}$  and label space  $\mathcal{Y}$  is a non trivial task. In particular, exact data forging involves solving a given system of linear equations, where each solution corresponds to a forged mini-batch  $B'$ . However, of the infinite, distinct, solutions that may exist, there are currently no known efficient techniques for finding solutions that correspond to a mini-batch that falls within the allowed domain  $\mathcal{X} \times \mathcal{Y}$ .

### A. Exact Data Forging

Within the classification context, we have a model, *i.e.*, parameterised function  $f_\theta : \mathcal{X} \rightarrow \mathcal{Y}$  and loss function  $\ell : \mathcal{Y} \times \mathcal{Y} \rightarrow \mathbb{R}$ . Exact data forging may be stated as the problem of finding two distinct mini-batches  $B, B' \in \mathcal{Z}^b$ , where  $\mathcal{Z} := \mathcal{X} \times \mathcal{Y}$ , such that  $\nabla_\theta \mathcal{L}(B) = \nabla_\theta \mathcal{L}(B')$ , where  $\mathcal{L}(B) = \frac{1}{b} \sum_{(\mathbf{x}, \mathbf{y}) \in B} \ell(f_\theta(\mathbf{x}), \mathbf{y})$ . We define distinct mini-batches as follows, ensuring that they differ in at least one training example:

**Definition 1** (Distinct mini-batches). *Two mini-batches  $B, B' \in \mathcal{Z}^b$  are distinct if  $\exists (\mathbf{x}, \mathbf{y}) \in B$  such that  $\forall (\mathbf{x}', \mathbf{y}') \in B', (\mathbf{x}, \mathbf{y}) \neq (\mathbf{x}', \mathbf{y}')$ .*

In the unrestricted setting, the training examples  $(\mathbf{x}, \mathbf{y}) \in B$  may take any real numbered value *i.e.*  $\mathcal{Z} = \mathbb{R}^d \times \mathbb{R}^n$  ( $d$  and  $n$  are the number of input features and classes respectively). However, depending on the given machine learning application, the domain may be restricted. Let us consider the image classification context, as done in the prior work, where inputs consist of pixel values and the labels are one hot vectors. There exist a finite number of pixel values  $v$  and  $n$  possible one hot vectors. Modern image formats have  $v = 256$ , so the domain of possible mini-batches is restricted to the set  $\mathcal{Z} = \{ \frac{q}{255} : q \in [0..255] \}^d \times \{u \in \{0, 1\}^n : \sum_{i=1}^n u_i = 1\}$ . We see that this domain is finite, and so one potential exact data forging approach is to enumerate every possible batch and search exhaustively for the one that produces the required gradient. However, this approach is computationally intractable for non-trivial values of  $b, d$  and  $n$  with no additional guarantee that one may be found<sup>7</sup> (see Appendix B for how exact data forging fails for small values of  $b, d, v$  and  $n$ ). Next we consider the task of exact data forging fully connected neural networks first for  $b = 1$ , and then consider the case for  $b > 1$ .

### B. Case for $b = 1$

For  $b = 1$  we prove that data forging is indeed not possible for fully connected neural networks. A  $L$ -layer fully connected neural network is made up of parameters that

<sup>7</sup>There exist a total of  $\binom{256^d \times n}{b}$  possible mini-batches of size  $b$ .

consist of weights and biases  $\theta = [\mathbf{W}_1, \mathbf{b}_1 \mathbf{W}_2, \mathbf{b}_2, \dots, \mathbf{W}_L, \mathbf{b}_L]$  where each  $\mathbf{W}_i \in \mathbb{R}^{d_{i-1} \times d_i}$ ,  $\mathbf{b} \in \mathbb{R}^{d_i}$ . The output of the neural network is given by  $f_\theta(\mathbf{x}) = \text{softmax}(\mathbf{z}_L)$ , where  $\mathbf{z}_L = \mathbf{W}_L^T \mathbf{a}_{L-1} + \mathbf{b}_L$ ,  $\mathbf{a}_i = h(\mathbf{z}_i)$ ,  $\mathbf{z}_i = \mathbf{W}_i^T \mathbf{a}_{i-1} + \mathbf{b}_i$ , and  $h$  is the activation function. Let  $n = d_L$  denote the number of classes,  $d = d_0$  the number of input features, and  $\mathbf{a}_0 = \mathbf{x} \in \mathbb{R}^d$ . The per example crossentropy loss  $\ell$  is given by  $\ell(\hat{\mathbf{y}}, \mathbf{y}) = -\sum_{i=1}^n y_i \log \hat{y}_i$ . Observe in the  $L = 1$  case, the network is equivalent to multi-class logistic regression.

**Proposition 1** ( $b = 1$  Data Forging Fully Connected Neural Networks). *Let  $\mathcal{Z} := \mathbb{R}^d \times \{u \in \{0, 1\}^n : \sum_{i=1}^n u_i = 1\}$ . For any two training examples  $(\mathbf{x}, \mathbf{y}), (\mathbf{x}', \mathbf{y}') \in \mathcal{Z}$  if  $\nabla_\theta \ell(f_\theta(\mathbf{x}), \mathbf{y}) = \nabla_\theta \ell(f_\theta(\mathbf{x}'), \mathbf{y}')$ , then  $\mathbf{x} = \mathbf{x}'$  and  $\mathbf{y} = \mathbf{y}'$ .*

Proposition 1 states that no two distinct training examples with one hot labels can produce the same gradient, an intuitive result and one that may point towards the difficulty of exact data forging. Further, proposition 1 proves the stronger result of impossibility of exact data forging when  $b = 1$  for distinct inputs in the infinite domain  $\mathbf{x}, \mathbf{x}' \in \mathbb{R}^d$ , not just the finite set of valid discrete-valued images (see appendix A1 for the full proof). However, models are typically trained with a batch size  $b \gg 1$ , therefore an investigation of the possibility of data forging within this regime is required.

### C. Case of $b > 1$

In contrast to the previous setting, we prove that there can exist distinct mini-batches of size  $b > 1$  that produce the same gradient.

**Proposition 2** ( $b > 1$  Data Forging Fully Connected Neural Networks). *Given a fully connected neural network and mini-batch  $B = \{(\mathbf{x}^{(k)}, \mathbf{y}^{(k)})\}_{k=1}^b$ , if  $db > d_1(d + b)$ , where  $d_1$  is the size of the first hidden layer, then there exists an infinite number of perturbation matrices  $\mathbf{P} \in \mathbb{R}^{d \times b}$  such that for the distinct mini-batch  $B' = \{(\mathbf{x}^{(k)} + [\mathbf{P}]^k, \mathbf{y}^{(k)})\}_{k=1}^b$ ,  $\nabla_\theta \mathcal{L}(B) = \nabla_\theta \mathcal{L}(B')$ .*

Proposition 2 proves the existence of perturbations that can be applied to the original training examples  $(\mathbf{x}, \mathbf{y}) \in B$  such that the same gradient is still preserved (see Fig. 4 for an example). For simplicity, we describe the construction of these perturbations in the case of a  $L = 1$  layer network with no bias (see appendix A3 for a full proof of proposition 2 and description of the construction of these perturbations for arbitrary depth fully connected neural networks with or without biases).

Consider a  $L = 1$  network (i.e., equivalent to multi-class logistic regression) with a single parameter matrix  $\mathbf{W} \in \mathbb{R}^{d \times n}$ . Let  $\mathbf{X} \in \mathbb{R}^{d \times b}$  represent the input matrix for mini-batch  $B$  i.e., the  $k$ -th column of  $\mathbf{X}$  is the  $k$ -th training example input  $\mathbf{x}^{(k)}$  from  $B$ , let  $\mathbf{Y} \in \mathbb{R}^{n \times b}$  be the corresponding label matrix, and vector  $\mathbf{v} \in \mathbb{R}^b$  such that  $v_k = \sum_{i=1}^n y_i^{(k)}$ . Additionally, let  $f_{\mathbf{W}}(\mathbf{X}) = \text{softmax}(\mathbf{W}^T \mathbf{X})$  be the batched softmaxed output<sup>8</sup>

<sup>8</sup>Softmax is applied along the columns of  $\mathbf{W}^T \mathbf{X}$ .

of the model. For crossentropy loss, the gradient is given by  $\nabla_{\mathbf{W}} \mathcal{L}(B) = \frac{1}{b} \mathbf{X} (f_{\mathbf{W}}(\mathbf{X}) \text{diag}(\mathbf{v}) - \mathbf{Y})^T$ .

Exact data forging reduces to the problem of finding two matrices  $\mathbf{X}' \in \mathbb{R}^{d \times b}$ ,  $\mathbf{Y}' \in \mathbb{R}^{n \times b}$  where  $\mathbf{X}' \neq \mathbf{X}$  such that  $\mathbf{X} (f_{\mathbf{W}}(\mathbf{X}) \text{diag}(\mathbf{v}) - \mathbf{Y})^T = \mathbf{X}' (f_{\mathbf{W}}(\mathbf{X}') \text{diag}(\mathbf{v}') - \mathbf{Y}')^T$ . Having done so, the forged mini-batch  $B'$  may be constructed from the columns of  $\mathbf{X}'$  and  $\mathbf{Y}'$ , namely the  $k$ -th forged example  $\mathbf{x}'$  is the  $k$ -th column of  $\mathbf{X}'$ , and likewise for the labels.

The *mini-batch perturbation* approach to exact data forging produces forged mini-batches with the same labels as the original i.e.,  $\mathbf{Y}' := \mathbf{Y}$ , however we construct a distinct input matrix  $\mathbf{X}' \neq \mathbf{X}$ . In particular,  $\mathbf{X}'$  is to set  $\mathbf{X}' := \mathbf{X} + \mathbf{P}$ , where  $\mathbf{P} \in \mathbb{R}^{d \times b}$  is some non-zero matrix that *perturbs*  $\mathbf{X}$  in such a way that maintains the same gradient. For such a matrix to do so, it must satisfy the following equations

$$\begin{cases} \mathbf{W}^T \mathbf{P} = \mathbf{0} \\ \mathbf{P} (f_{\mathbf{W}}(\mathbf{X}) \text{diag}(\mathbf{v}) - \mathbf{Y})^T = \mathbf{0}. \end{cases} \quad (1)$$

If  $\mathbf{P}$  satisfies the first equation  $\mathbf{W}^T \mathbf{P} = \mathbf{0}$ , then  $f_{\mathbf{W}}(\mathbf{X}') = \text{softmax}(\mathbf{W}^T(\mathbf{X} + \mathbf{P})) = \text{softmax}(\mathbf{W}^T \mathbf{X} + \mathbf{W}^T \mathbf{P}) = \text{softmax}(\mathbf{W}^T \mathbf{X}) = f_{\mathbf{W}}(\mathbf{X})$ . In other words, satisfying the first equation ensures that the original and forged mini-batch produce the same output. If  $\mathbf{P}$  satisfies both equations, we then have

$$\begin{aligned} b \nabla_{\mathbf{W}} \mathcal{L}(B') &= \mathbf{X}' (f_{\mathbf{W}}(\mathbf{X}') \text{diag}(\mathbf{v}') - \mathbf{Y}')^T \\ &= (\mathbf{X} + \mathbf{P}) (f_{\mathbf{W}}(\mathbf{X}') \text{diag}(\mathbf{v}') - \mathbf{Y}')^T \\ &= (\mathbf{X} + \mathbf{P}) (f_{\mathbf{W}}(\mathbf{X}) \text{diag}(\mathbf{v}) - \mathbf{Y})^T \\ &= \mathbf{X} (f_{\mathbf{W}}(\mathbf{X}) \text{diag}(\mathbf{v}) - \mathbf{Y})^T + \mathbf{P} (f_{\mathbf{W}}(\mathbf{X}) \text{diag}(\mathbf{v}) - \mathbf{Y})^T \\ &= \mathbf{X} (f_{\mathbf{W}}(\mathbf{X}) \text{diag}(\mathbf{v}) - \mathbf{Y})^T = b \nabla_{\mathbf{W}} \mathcal{L}(B) \end{aligned} \quad (2)$$

Thus, satisfying the two equations given in 1 ensures that the gradients for the original and forged mini-batch match.

In order to construct  $\mathbf{P}$ , we first observe that we can write the two equations as  $\mathbf{I}_d \mathbf{P} \mathbf{D} = \mathbf{0}$  and  $\mathbf{W}^T \mathbf{P} \mathbf{I}_b = \mathbf{0}$ , where  $\mathbf{I}_k$  is the identity matrix of size  $k$ , and  $\mathbf{D} = (f_{\mathbf{W}}(\mathbf{X}) \text{diag}(\mathbf{v}) - \mathbf{Y})^T$ . Using the identity  $AXB = C \iff (B^T \otimes A) \text{vec}(X) = \text{vec}(C)$ , we can then rewrite our two equations as their corresponding linear systems and combine them into the following single system of linear equations:

$$\begin{bmatrix} \mathbf{D}^T \otimes \mathbf{I}_d \\ \mathbf{I}_b \otimes \mathbf{W}^T \end{bmatrix} \text{vec}(\mathbf{P}) = \mathbf{0} \quad (3)$$

Let  $\mathbf{K} \in \mathbb{R}^{n(b+d) \times bd}$  be the above coefficient matrix, then the general solution is given by:

$$\text{vec}(\mathbf{P}) = (\mathbf{I} - \mathbf{K}^+ \mathbf{K}) \mathbf{F}, \quad (4)$$

where  $\mathbf{F} \in \mathbb{R}^{bd}$  is an arbitrary column matrix, and  $\mathbf{K}^+$  is the psuedo-inverse of  $\mathbf{K}$ .

For the homogenous linear system  $\mathbf{K} \text{vec}(\mathbf{P}) = \mathbf{0}$ , there are  $bd - \text{rank}(\mathbf{K})$  linearly independent solutions. If  $\mathbf{K}$  is full rank and square, there are no non-trivial solutions. In order to ensure at least 1 set of linearly dependent solutions (e.g.

one free variable)  $bd > n(b + d)$  must hold. This ensures that  $bd - \text{rank}(\mathbf{K}) \geq 1$ . This is a worst case condition on the existence of non-trivial solutions as  $\mathbf{K}$  may not necessarily be full rank.



Fig. 4: **Bottom:** The original mini-batch  $B$  consisting of  $b = 32$  examples from MNIST. **Top:** A forged mini-batch  $B'$  with an approximation error of  $\approx 10^{-7}$ . In this setting, the model is an  $L = 2$  ReLU neural network with 8 hidden units. Similar mini-batches were constructed by Pan et al. [17] within the context of gradient inversion.

Exact data forging can be performed using this *mini-batch perturbation* approach; see Figure 4 for an example. However, while the gradients match, the forged input examples  $\mathbf{x}'^{(k)}$  are not guaranteed to be members of the set of valid images  $\{\frac{q}{255}, q \in [0..255]\}^d$ ; the applied perturbation may result in a mini-batch that is outside the allowed input domain. In order to ensure this does not happen, one needs to find one of the infinitely many possible perturbations **i.e.**, solutions to equation (4), that preserves image validity. This requires choosing the correct arbitrary column matrix  $\mathbf{F}$ . Efficiently finding this matrix is a non trivial task, and is currently the main barrier to successful exact data forging. In fact, the question of whether such matrices may exist is also still unresolved, even for relatively simple linear models.

#### D. Exact Data Forging for $L = 1$ Networks

Recall earlier that for a  $L = 1$  network with single parameter matrix  $\mathbf{W}$ , the gradient of crossentropy loss is given by  $\nabla_{\mathbf{W}}\mathcal{L}(B) = \frac{1}{b}\mathbf{X}(f_{\mathbf{W}}(\mathbf{X})\text{diag}(\mathbf{v}) - \mathbf{Y})^T$ , and that exact data forging reduces to the problem of finding two matrices  $\mathbf{X}' \in \mathbb{R}^{d \times b}, \mathbf{Y}' \in \mathbb{R}^{n \times b}$  where  $\mathbf{X}' \neq \mathbf{X}$  such that  $\mathbf{X}(f_{\mathbf{W}}(\mathbf{X})\text{diag}(\mathbf{v}) - \mathbf{Y})^T = \mathbf{X}'(f_{\mathbf{W}}(\mathbf{X}')\text{diag}(\mathbf{v}') - \mathbf{Y}')^T$ .

**Proposition 3** ( $L = 1$  Data Forging). *If  $b > \text{rank}(\nabla_{\mathbf{W}}\mathcal{L}(B))$ , then there exists an infinite number of distinct mini-batches  $B' \subset \mathbb{R}^d \times \mathbb{R}^n$  of size  $b$  such that  $\nabla_{\mathbf{W}}\mathcal{L}(B') = \nabla_{\mathbf{W}}\mathcal{L}(B)$ .*

Proposition 3 (see appendix A4 for the proof) extends the mini-batch perturbation approach for  $L = 1$  networks, showing that there can exist two distinct mini-batches with the same gradient that are not necessarily a perturbation of the other, and do not share the same labels (see Fig. 5 for an example). We prove this with the following steps:

Let matrix  $\mathbf{D} = (f_{\mathbf{W}}(\mathbf{X})\text{diag}(\mathbf{v}) - \mathbf{Y})^T$  be the error matrix of the model on input  $\mathbf{X}$ . Our first method of exact data forging exploits a fundamental property of this matrix (for proof see Appendix 4).

**Lemma 1.** *Let  $\mathbf{D} = (f_{\mathbf{W}}(\mathbf{X})\text{diag}(\mathbf{v}) - \mathbf{Y})^T$ . For any two matrices  $\mathbf{X} \in \mathbb{R}^{d \times b}$  and  $\mathbf{Y} \in \mathbb{R}^{n \times b}$ , we have that  $\sum_{j=1}^n \mathbf{D}_{ij} = 0, \forall i, 1 \leq i \leq b$ .*

Using this property, we may devise the following *error matrix sampling* approach towards exact data forging for  $L = 1$  networks. Given mini-batch  $B$  of size  $b$  and gradient  $\nabla_{\mathbf{W}}\mathcal{L}(B)$  of rank  $r$ :

- 1) Sample any matrix  $\mathbf{D} \in \mathbb{R}^{b \times n}$  of such that  $\sum_{j=1}^n \mathbf{D}_{ij} = 0$  and  $\text{rank}(\mathbf{D}) \geq r$ .
- 2) Solve for  $\mathbf{X}'$  the matrix equation  $\mathbf{X}'\mathbf{D} = b\nabla_{\mathbf{W}}\mathcal{L}(B)$ .
- 3) Set  $\mathbf{Y}' := f_{\mathbf{W}}(\mathbf{X}')\text{diag}(\mathbf{v}) - \mathbf{D}^T$ .
- 4) Construct forged mini-batch  $B' = \{(\mathbf{x}'^{(k)}, \mathbf{y}'^{(k)})\}_{k=1}^b$  where each  $\mathbf{x}'^{(k)}, \mathbf{y}'^{(k)}$  are the  $k$ -th column of  $\mathbf{X}', \mathbf{Y}'$  respectively.

Figure 5 gives two such examples of distinct mini-batches that produce the same gradient for both the MNIST and CIFAR10 datasets for an  $L = 1$  network. The above error matrix sampling approach is not restricted to constructing forged mini-batches with the same labels as the original, proving the existence of distinct mini-batches with distinct labels can produce the same gradient. The infinite number of possible error matrices  $\mathbf{D}$  as well as the potentially infinite solutions to equation  $\mathbf{X}'\mathbf{D} = b\nabla_{\mathbf{W}}\mathcal{L}(B)$  capture all the distinct mini-batches  $B' \subset \mathbb{R}^d \times \mathbb{R}^n$  such that  $\nabla_{\mathbf{W}}\mathcal{L}(B) = \nabla_{\mathbf{W}}\mathcal{L}(B')$ . However, analogous to the mini-batch perturbation approach, choosing the correct error matrix  $\mathbf{D}$  such that the mini-batch  $B'$  that is constructed from the resulting  $\mathbf{X}'$  and  $\mathbf{Y}'$  falls within the required domain is a non trivial, computationally infeasible task.

Our analysis takes the first step towards understanding exact data forging. Within the unrestricted mini-batch domain, we prove that exact data forging is indeed possible and provide methods of constructing forged mini-batches with approximation errors that are indistinguishable from reproduction errors. Further research and analysis are required in order to determine whether data forging within these restricted domains is possible. Given the difficulty of this task, we conjecture that it may not be computationally feasible.

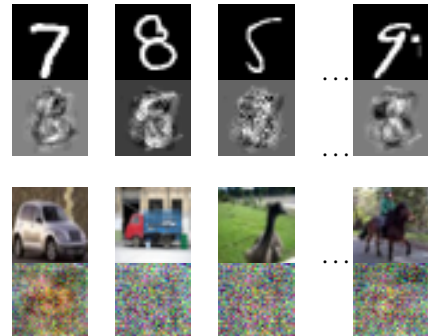


Fig. 5: A mini-batch from MNIST (top) and CIFAR10 (bottom) and distinct forged counterpart produced by our error matrix sampling approach. Both examples produce an approximation error on the order of  $10^{-7}$ , 5 orders of magnitude smaller than existing attacks.

## VII. RELATED WORK

We review two primary lines of related research: (i) the concept of proof of learning in ML and (ii) the construction of PoL adversarial examples.

### A. Proof of Learning

Jia et al. [11] observed that the production and verification of an execution trace is tantamount to proving one has trained model  $\theta_T$  on dataset  $D = \bigcup_{i=0}^{T-1} B_i$ . They formalise execution traces as *Proof of Learning* (PoL) sequences, and verify the final model  $\theta_T$  is indeed the result of the optimisation captured in the trace by recomputing the checkpoints using the provided mini-batches and previous checkpoint, ensuring that each recomputed checkpoint is within some pre-defined distance threshold  $\epsilon$ , e.g.  $\ell_2$  norm, from what is reported in the trace.

Implicit within the definition of PoL is the uniqueness of execution traces for a given final model  $\theta_T$ , and that the construction of a distinct trace for  $\theta_T$  that passes verification is at least as difficult a task as training. Consequently, Jia et al. consider PoL as a viable means of proving a third party has indeed expended the energy to train the model and therefore owns it. Constructing distinct traces that challenge this assumption is known as PoL “spoofing”, i.e., producing a trace that differs from the original by employing a different sequence of mini-batches that follow a different training trajectory, but ultimately end at the same final model  $\theta_T$ . Given such a spoofed execution trace  $S'$  for original trace  $S$ , let  $D$  and  $D'$  be the differing datasets used in  $S$  and  $S'$  respectively. One immediate consequence of successful PoL spoofing regards the training examples  $(\mathbf{x}, \mathbf{y}) \notin D \cap D'$ ; namely the question arises of “*which are the real training examples that trained  $\theta_T$ ?*” PoL spoofing results in the apparent contradiction that a model was both trained and not trained on some set of training examples, in effect *deleting* them from a model’s training set.

### B. PoL Adversarial Examples

Zhang et al. [30] challenged the underlying assumption of PoL by constructing “adversarial examples” to PoL *i.e.*, two distinct execution traces for the same final model  $\theta_T$ . Zhang et al.’s proposed adversarial attack operates by initialising dummy checkpoints such that the distance between consecutive checkpoints is less than the chosen verification distance threshold  $\epsilon$ , and optimise “random” noise to add to mini-batches consisting of public data such that the gradient is close to zero, ensuring the next model checkpoint lies within the  $\epsilon$ -ball of the next dummy checkpoint, and thus passing verification. However, Fang et al. [8] find that they are fragile to the hyperparameters of the verification process. Namely, under small checkpointing intervals, the attacks break down. Additionally, Zhang et al. apply their attack to image classification models, and there is no mention nor guarantee of whether the final synthesized images are still within the problem domain *e.g.*, whether the final pixel values are within  $0 - 255$ . Any training examples outside the problem domain in the mini-batches of an execution trace immediately point

to a detectable spoof. Fang et al. provide an “infinitesimal update” attack against PoL that is conceptually similar to Zhang et al.’s, where a learning rate is chosen to be sufficiently small such that regardless of the training data, the next model checkpoint lies within the  $\epsilon$ -ball of the dummy checkpoint. The success of these attacks that exploit the static verification threshold and their consequences on the robustness of PoL verification is discussed in [8]. One limitation of these attacks is that they require foreknowledge of the chosen  $\epsilon$  by the verifier, something that may not be realistic in practice, and the utilisation of infinitesimally small learning rates may also be suspect to a verifier.

Existing PoL adversarial attacks [30], [8] exploit near zero norm gradients to produce distinct execution traces that can pass PoL verification. However it remains an open question whether two distinct execution traces with distinct checkpoints may be constructed for model  $\theta_T$  with valid, honest gradient updates that do not require near zero norm gradients. Fang et al. evaluate attempts at doing so via data ordering attacks [21] *i.e.*, finding a distinct sequence of valid mini-batches that take random initialisation  $\theta_0$  to the desired  $\theta_T$ ; however these were also found to be unlikely to succeed.

## VIII. CONCLUSION

Answers to the question of exact data forging within the restricted problem domain will have wide reaching ramifications for the machine learning and privacy community. Proving its feasibility and the development of methods of performing such a task allows for stealthy data forging; an attack which fully realises the serious data privacy and security implications recognised by the prior work [12], [23], [29]. Membership inference attacks are the bread-and-butter of machine learning privacy. They are used to perform ML auditing and compliance, two tasks that are key in any real world deployment of an ML model. Additionally, machine unlearning is currently the only adequate response to GDPR’s *right to be forgotten*, allowing model owners to comply with the law without needing to throw away the entire model. Stealthy data forging has the potential to disrupt these two tools, casting doubt on their methodology and veracity. These are serious implications for the ML privacy community, however, they have not been fully realised by current data forging attacks. Further research is needed on whether stealthy data forging is indeed possible; and whether more powerful attack algorithms exist. We have begun by first conclusively determining that current attacks are not stealthy and are detectable, cancelling any implications they may have on ML privacy. Additionally, our theoretical analysis takes a first step towards understanding data forging and analysing the conditions where different mini-batches can produce the same update.

## REFERENCES

[1] Gradient-based learning applied to document recognition. *Proceedings of the IEEE*, 86(11):2278–2324, 1998.

[2] Martín Abadi, Paul Barham, Jianmin Chen, Zhifeng Chen, Andy Davis, Jeffrey Dean, Matthieu Devin, Sanjay Ghemawat, Geoffrey Irving, Michael Isard, et al. {TensorFlow}: a system for {Large-Scale} machine learning. In *12th USENIX symposium on operating systems design and implementation (OSDI 16)*, pages 265–283, 2016.

[3] Teodora Baluta, Ivica Nikolic, Racchit Jain, Divesh Aggarwal, and Prateek Saxena. Unforgeability in stochastic gradient descent. In *Proceedings of the 2023 ACM SIGSAC Conference on Computer and Communications Security*, pages 1138–1152, 2023.

[4] Lucas Bourtoule, Varun Chandrasekaran, Christopher A Choquette-Choo, Hengrui Jia, Adelin Travers, Baiwu Zhang, David Lie, and Nicolas Papernot. Machine unlearning. In *2021 IEEE Symposium on Security and Privacy (SP)*, pages 141–159. IEEE, 2021.

[5] Yinzhi Cao and Junfeng Yang. Towards making systems forget with machine unlearning. In *2015 IEEE symposium on security and privacy*, pages 463–480. IEEE, 2015.

[6] Nicholas Carlini, Steve Chien, Milad Nasr, Shuang Song, Andreas Terzis, and Florian Tramer. Membership inference attacks from first principles. In *2022 IEEE Symposium on Security and Privacy (SP)*, pages 1897–1914. IEEE, 2022.

[7] Cynthia Dwork. Differential privacy. In *International colloquium on automata, languages, and programming*, pages 1–12. Springer, 2006.

[8] Congyu Fang, Hengrui Jia, Anvith Thudi, Mohammad Yaghini, Christopher A Choquette-Choo, Natalie Dullerud, Varun Chandrasekaran, and Nicolas Papernot. Proof-of-learning is currently more broken than you think. In *2023 IEEE 8th European Symposium on Security and Privacy (EuroS&P)*, pages 797–816. IEEE, 2023.

[9] Scott Grauer-Gray, Lifan Xu, Robert Searles, Sudhee Ayalasomayajula, and John Cavazos. Auto-tuning a high-level language targeted to gpu codes. In *2012 innovative parallel computing (InPar)*, pages 1–10. Ieee, 2012.

[10] Hongsheng Hu, Zoran Salcic, Lichao Sun, Gillian Dobbie, Philip S. Yu, and Xuyun Zhang. Membership inference attacks on machine learning: A survey. *ACM Comput. Surv.*, 54(11s), sep 2022.

[11] Hengrui Jia, Mohammad Yaghini, Christopher A Choquette-Choo, Natalie Dullerud, Anvith Thudi, Varun Chandrasekaran, and Nicolas Papernot. Proof-of-learning: Definitions and practice. In *2021 IEEE Symposium on Security and Privacy (SP)*, pages 1039–1056. IEEE, 2021.

[12] Zhifeng Kong, Amrita Roy Chowdhury, and Kamalika Chaudhuri. Can membership inferencing be refuted? *arXiv preprint arXiv:2303.03648*, 2023.

[13] Alex Krizhevsky, Vinod Nair, and Geoffrey Hinton. Cifar-10 (canadian institute for advanced research). *URL <http://www.cs.toronto.edu/~kriz/cifar.html>*, 5(4):1, 2010.

[14] Yann LeCun. The mnist database of handwritten digits. *<http://yann.lecun.com/exdb/mnist/>*, 1998.

[15] California Legislature. California consumer privacy act (ccpa), 2018. California Civil Code §§ 1798.100 - 1798.199.

[16] Brendan McMahan, Eider Moore, Daniel Ramage, Seth Hampson, and Blaise Aguera y Arcas. Communication-efficient learning of deep networks from decentralized data. In *Artificial intelligence and statistics*, pages 1273–1282. PMLR, 2017.

[17] Xudong Pan, Mi Zhang, Yifan Yan, Jiaming Zhu, and Zhemin Yang. Exploring the security boundary of data reconstruction via neuron exclusivity analysis. In *31st USENIX Security Symposium (USENIX Security 22)*, pages 3989–4006, 2022.

[18] Adam Paszke, Sam Gross, Francisco Massa, Adam Lerer, James Bradbury, Gregory Chanan, Trevor Killeen, Zeming Lin, Natalia Gimelshein, Luca Antiga, et al. Pytorch: An imperative style, high-performance deep learning library. *Advances in neural information processing systems*, 32, 2019.

[19] Alexander Schögl, Nora Hofer, and Rainer Böhme. Causes and effects of unanticipated numerical deviations in neural network inference frameworks. In *Thirty-seventh Conference on Neural Information Processing Systems*, 2023.

[20] Reza Shokri, Marco Stronati, Congzheng Song, and Vitaly Shmatikov. Membership inference attacks against machine learning models. In *2017 IEEE symposium on security and privacy (SP)*, pages 3–18. IEEE, 2017.

[21] Ilia Shumailov, Zakhar Shumaylov, Dmitry Kazhdan, Yiren Zhao, Nicolas Papernot, Murat A Erdogan, and Ross J Anderson. Manipulating sgd with data ordering attacks. *Advances in Neural Information Processing Systems*, 34:18021–18032, 2021.

[22] Karen Simonyan and Andrew Zisserman. Very deep convolutional networks for large-scale image recognition. *arXiv preprint arXiv:1409.1556*, 2014.

[23] Anvith Thudi, Hengrui Jia, Ilia Shumailov, and Nicolas Papernot. On the necessity of auditable algorithmic definitions for machine unlearning. In *31st USENIX Security Symposium (USENIX Security 22)*, pages 4007–4022, 2022.

[24] European Union. General data protection regulation (gdpr), 2016. Regulation (EU) 2016/679 of the European Parliament and of the Council of 27 April 2016.

[25] Paul Voigt and Axel Von dem Bussche. The eu general data protection regulation (gdpr). *A Practical Guide, 1st Ed.*, Cham: Springer International Publishing, 10(3152676):10–5555, 2017.

[26] Heng Xu, Tianqing Zhu, Lefeng Zhang, Wanlei Zhou, and Philip S Yu. Machine unlearning: A survey. *ACM Computing Surveys*, 56(1):1–36, 2023.

[27] Haomiao Yang, Mengyu Ge, Dongyun Xue, Kunlan Xiang, Hongwei Li, and Rongxing Lu. Gradient leakage attacks in federated learning: Research frontiers, taxonomy and future directions. *IEEE Network*, pages 1–8, 2023.

[28] H. Yin, A. Mallya, A. Vahdat, J. M. Alvarez, J. Kautz, and P. Molchanov. See through gradients: Image batch recovery via gradinversion. In *2021 IEEE/CVF Conference on Computer Vision and Pattern Recognition (CVPR)*, pages 16332–16341, Los Alamitos, CA, USA, jun 2021. IEEE Computer Society.

[29] Binchi Zhang, Zihan Chen, Cong Shen, and Jundong Li. Verification of machine unlearning is fragile. In *Forty-first International Conference on Machine Learning*, 2024.

[30] Rui Zhang, Jian Liu, Yuan Ding, Zhibo Wang, Qingbiao Wu, and Kui Ren. “adversarial examples” for proof-of-learning. In *2022 IEEE Symposium on Security and Privacy (SP)*, pages 1408–1422. IEEE, 2022.

[31] Bo Zhao, Konda Reddy Mopuri, and Hakan Bilen. idlg: Improved deep leakage from gradients, 2020.

[32] Junyi Zhu and Matthew Blaschko. R-gap: Recursive gradient attack on privacy. *Proceedings ICLR 2021*, 2021.

[33] Ligeng Zhu, Zhijian Liu, and Song Han. Deep leakage from gradients. In H. Wallach, H. Larochelle, A. Beygelzimer, F. d’Alché-Buc, E. Fox, and R. Garnett, editors, *Advances in Neural Information Processing Systems*, volume 32. Curran Associates, Inc., 2019.

## APPENDIX

### A. Proofs

1) **Proof of Proposition 1:** We first introduce the background, namely the neural network setup, the definition of the loss function, and derive expressions for the gradients of the loss function with respect to the network parameters. Then, we introduce and prove some lemmas that are needed for the full proof. Finally the full proof is given.

**Background.** A  $L$ -layer fully connected neural network consists of weights and biases  $\theta = [\mathbf{W}_1, \mathbf{b}_1 \mathbf{W}_2, \mathbf{b}_2, \dots, \mathbf{W}_L, \mathbf{b}_L]$  where each  $\mathbf{W}_i \in \mathbb{R}^{d_{i-1} \times d_i}$ ,  $\mathbf{b} \in \mathbb{R}^{d_i}$ . The output of the neural network is given by  $f_\theta(\mathbf{x}) = \text{softmax}(\mathbf{z}_L)$ , where  $\mathbf{z}_L = \mathbf{W}_L^T \mathbf{a}_{L-1} + \mathbf{b}_L$ ,  $\mathbf{a}_i = h(\mathbf{z}_i)$ ,  $\mathbf{z}_i = \mathbf{W}_i^T \mathbf{a}_{i-1} + \mathbf{b}_i$ , and  $h$  is the activation function. Let  $n = d_L$  denote the number of classes,  $d = d_0$  the number of input features, and  $\mathbf{a}_0 = \mathbf{x} \in \mathbb{R}^d$ . The per example crossentropy loss  $\ell$  is given by  $\ell(\hat{\mathbf{y}}, \mathbf{y}) = -\sum_{i=1}^n y_i \log \hat{y}_i$ . Observe in the  $L = 1$  case, the network is equivalent to multi-class logistic regression.  $\nabla_{\mathbf{W}_i} \ell$  is given by the outer product of the vectors  $\mathbf{a}_{i-1}$  and  $\delta_i$ :

$$\nabla_{\mathbf{W}_i} \ell = \mathbf{a}_{i-1} \delta_i^T \quad (5)$$

where  $\delta_i = \frac{\partial \ell}{\partial \mathbf{z}_i} \in \mathbb{R}^{d_i}$ . Additionally,  $\nabla_{\mathbf{b}_i} \ell = \delta_i$ . We have that

$$\delta_i = \text{diag}(\mathbf{h}_i) \mathbf{W}_{i+1} \delta_{i+1}, \quad (6)$$

where  $\mathbf{h}_i = [h'(z_1^{(i)}), \dots, h'(z_{d_i}^{(i)})]^T \in \mathbb{R}^{d_i}$ . Let  $z_j = [\mathbf{z}_L]_j$ ,  $y_i = [\mathbf{y}]_i$  and  $\hat{y}_j = [f_\theta(\mathbf{x})]_j$ . We can write the  $j$ -th element of  $\delta_L$  as the following:

$$\begin{aligned} [\delta_L]_j &= \frac{\partial \ell}{\partial z_j} = -\sum_{i=1}^n y_i \cdot \frac{\partial \log \hat{y}_i}{\partial z_j} \\ &= -\sum_{i=1}^n \frac{y_i}{\hat{y}_i} \cdot \frac{\partial \hat{y}_i}{\partial z_j} \end{aligned} \quad (7)$$

We know that the derivative of the softmax function is given by

$$\frac{\partial \hat{y}_i}{\partial z_j} = \begin{cases} \hat{y}_j(1 - \hat{y}_j) & \text{if } i = j \\ -\hat{y}_i \cdot \hat{y}_j & \text{otherwise,} \end{cases} \quad (8)$$

which allows us to rewrite Equation 7 as

$$\begin{aligned} [\delta_L]_j &= \frac{\partial \ell}{\partial z_j} = -y_j(1 - \hat{y}_j) - \sum_{\substack{i=1 \\ i \neq j}}^n y_i \cdot (-\hat{y}_j) \\ &= -y_j + \hat{y}_j \sum_{i=1}^n y_i \end{aligned} \quad (9)$$

From (9), we have that  $\delta_L = v\hat{\mathbf{y}} - \mathbf{y}$ , where  $v = \sum_{i=1}^n [\mathbf{y}]_i$ .

### Associated Lemmas and Corollaries

**Lemma 2.** For any two training examples  $(\mathbf{x}, \mathbf{y})$  and  $(\mathbf{x}', \mathbf{y}')$ , if  $\nabla_{\mathbf{W}_1} \ell(\mathbf{x}', \mathbf{y}') = \nabla_{\mathbf{W}_1} \ell(\mathbf{x}, \mathbf{y})$  and  $\nabla_{\mathbf{b}_1} \ell(\mathbf{x}', \mathbf{y}') = \nabla_{\mathbf{b}_1} \ell(\mathbf{x}, \mathbf{y})$ , then  $\mathbf{x} = \mathbf{x}'$ .

*Proof.* If  $\nabla_{\mathbf{W}_1} \ell(\mathbf{x}', \mathbf{y}') = \nabla_{\mathbf{W}_1} \ell(\mathbf{x}, \mathbf{y})$ , then  $\mathbf{x}' \delta_1'^T = \mathbf{x} \delta_1^T$ . If  $\nabla_{\mathbf{b}_1} \ell(\mathbf{x}', \mathbf{y}') = \nabla_{\mathbf{b}_1} \ell(\mathbf{x}, \mathbf{y})$ , then  $\delta_1' = \delta_1$ , resulting in the equation

$$\mathbf{x}' \mathbf{u}^T = \mathbf{x} \mathbf{u}^T \quad (10)$$

where  $\mathbf{u} = \delta_1' = \delta_1$ . Since we have an outer product, (10) is only satisfied when  $\mathbf{x} = \mathbf{x}'$ .  $\square$

**Lemma 3.** For any two training examples  $(\mathbf{x}, \mathbf{y})$  and  $(\mathbf{x}', \mathbf{y}')$ , if  $\nabla_{\mathbf{W}_L} \ell(\mathbf{x}', \mathbf{y}') = \nabla_{\mathbf{W}_L} \ell(\mathbf{x}, \mathbf{y})$  and  $\nabla_{\mathbf{b}_L} \ell(\mathbf{x}', \mathbf{y}') = \nabla_{\mathbf{b}_L} \ell(\mathbf{x}, \mathbf{y})$  then  $\mathbf{y} = (v - v')\mathbf{u} + \mathbf{y}'$ , where  $v = \sum_j [\mathbf{y}]_j$ ,  $v' = \sum_j [\mathbf{y}']_j$ , and  $\mathbf{u} \in \mathbb{R}^n$ .

*Proof.* If  $\nabla_{\mathbf{b}_L} \ell(\mathbf{x}', \mathbf{y}') = \nabla_{\mathbf{b}_L} \ell(\mathbf{x}, \mathbf{y})$ , then  $\delta_L' = \delta_L$ . If,  $\nabla_{\mathbf{W}_L} \ell(\mathbf{x}', \mathbf{y}') = \nabla_{\mathbf{W}_L} \ell(\mathbf{x}, \mathbf{y})$ , then

$$\mathbf{a}'_{L-1} \delta_L'^T = \mathbf{a}_{L-1} \delta_L^T \quad (11)$$

Since  $\delta'_L = \delta_L$  we have that  $\mathbf{a}'_{L-1} = \mathbf{a}_{L-1}$  for (11) to hold. Therefore,  $\mathbf{z}'_L = \mathbf{W}_L^T \mathbf{a}_{L-1} + \mathbf{b}_L = \mathbf{W}_L^T \mathbf{a}'_{L-1} + \mathbf{b}_L = \mathbf{z}_L$ . Therefore  $\hat{\mathbf{y}}' = \hat{\mathbf{y}}$ . Let  $\mathbf{u} = \hat{\mathbf{y}}' = \hat{\mathbf{y}}$ . Then

$$\begin{aligned}\delta'_L &= \delta_L \\ v' \hat{\mathbf{y}}' - \mathbf{y}' &= v \hat{\mathbf{y}} - \mathbf{y} \\ v' \mathbf{u} - \mathbf{y}' &= v \mathbf{u} - \mathbf{y} \\ \mathbf{y} &= (v - v') \mathbf{u} + \mathbf{y}'\end{aligned}\tag{12}$$

□

**Corollary 1.** For any two training examples  $(\mathbf{x}, \mathbf{y})$  and  $(\mathbf{x}', \mathbf{y}')$ , if  $\nabla_{\mathbf{W}_L} \ell(\mathbf{x}', \mathbf{y}') = \nabla_{\mathbf{W}_L} \ell(\mathbf{x}, \mathbf{y})$  and  $\nabla_{\mathbf{b}_L} \ell(\mathbf{x}', \mathbf{y}') = \nabla_{\mathbf{b}_L} \ell(\mathbf{x}, \mathbf{y})$  and  $\sum_j [\mathbf{y}]_j = \sum_j [\mathbf{y}']_j$  then  $\mathbf{y} = \mathbf{y}'$ .

*Proof.* If the first two conditions hold, then, by Lemma 3,  $\mathbf{y} = (v - v') \mathbf{u} + \mathbf{y}'$ , where  $v = \sum_j [\mathbf{y}]_j$ ,  $v' = \sum_j [\mathbf{y}']_j$ . If these two sums are equal, we then have that

$$\begin{aligned}\mathbf{y} &= (v - v') \mathbf{u} + \mathbf{y}' \\ \mathbf{y} &= (v - v) \mathbf{u} + \mathbf{y}' \\ \mathbf{y} &= \mathbf{y}'\end{aligned}\tag{13}$$

□

**Full Proof.** We now prove Proposition 1.

*Proof.* The proof follows from Lemma 2 and Lemma 3. From Lemma 2, if  $\nabla_{\mathbf{W}_1} \ell(\mathbf{x}', \mathbf{y}') = \nabla_{\mathbf{W}_1} \ell(\mathbf{x}, \mathbf{y})$  and  $\nabla_{\mathbf{b}_1} \ell(\mathbf{x}', \mathbf{y}') = \nabla_{\mathbf{b}_1} \ell(\mathbf{x}, \mathbf{y})$ , then  $\mathbf{x} = \mathbf{x}'$ .

From Lemma 3, if  $\nabla_{\mathbf{W}_L} \ell(\mathbf{x}', \mathbf{y}') = \nabla_{\mathbf{W}_L} \ell(\mathbf{x}, \mathbf{y})$  and  $\nabla_{\mathbf{b}_L} \ell(\mathbf{x}', \mathbf{y}') = \nabla_{\mathbf{b}_L} \ell(\mathbf{x}, \mathbf{y})$ , then  $\mathbf{y} = (v - v') \mathbf{u} + \mathbf{y}'$ . If  $\mathbf{y}$  and  $\mathbf{y}'$  are one hot labels, then  $v = v' = 1$ . Consequently, from Corollary 1,  $\mathbf{y} = \mathbf{y}'$ .

□

## 2) Proof of Lemma 1:

*Proof.* Let  $\mathbf{y} = [y_1, y_2, \dots, y_n]^T$  represent the  $i$ -th column of  $\mathbf{Y}$ , and  $\mathbf{s} = [s_1, s_2, \dots, s_n]^T$  represent the  $i$ -th column of  $f_{\mathbf{W}}(\mathbf{X})$ . We then have that

$$\begin{aligned}\sum_{j=1}^n D_{ij} &= \sum_{j=1}^n -y_j + s_j \sum_{k=1}^n y_k \\ &= -\sum_{j=1}^n y_j + \sum_{j=1}^n s_j \cdot \sum_{k=1}^n y_k \\ &= -\sum_{j=1}^n y_j + \sum_{k=1}^n y_k = 0.\end{aligned}\tag{14}$$

□

**3) Proof of Proposition 2:** We present the proof as follows: first we derive expressions for the gradient of the average loss function  $\nabla \mathcal{L}$  for fully connected neural networks, as done similarly in Appendix A1 for  $\nabla \ell$ . We then go on to give the full proof.

**Background.** For the mini-batch setting, we can derive matrix expressions for  $\nabla_{\mathbf{W}_i} \mathcal{L}$ . Writing everything in matrix notation, we have the input matrix  $\mathbf{X} \in \mathbb{R}^{d_0 \times b}$ , where the  $k$ -th column denotes  $\mathbf{x}^{(k)}$ . We can also write the batched output of the model  $\mathbf{Z}_L \in \mathbb{R}^{d_L \times b}$  as the following matrix multiplication:

$$\mathbf{Z}_L = \mathbf{W}_L^T \mathbf{A}_{L-1} + \mathbf{B}_L, \tag{15}$$

where each  $\mathbf{A}_i \in \mathbb{R}^{d_i \times b}$  is the batched activation after the  $i$ -th layer i.e., the  $k$ -th column of  $\mathbf{A}_i$  represents the activation of the network after the  $i$ -th layer for the  $k$ -th example in the mini-batch  $\mathbf{a}_i^{(k)} := [a_1^{(k,i)} a_2^{(k,i)} \dots a_{d_i}^{(k,i)}]^T$ :

$$\begin{aligned}\mathbf{A}_i &= h(\mathbf{Z}_i) \\ &= h(\mathbf{W}_i^T \mathbf{A}_{i-1} + \mathbf{B}_i),\end{aligned}\tag{16}$$

where  $\mathbf{A}_0 = \mathbf{X}$ , and  $\mathbf{B}_i \in \mathbb{R}^{d_i \times b}$ , which is a matrix where each of the columns are the same bias vector for the  $i$ -th layer repeated. Let the scalar  $z_m^{(k,i)}$  represents the the  $m$ -th logit value at the  $i$ -th layer of the  $k$ -th training example in the mini-batch, and let the scalar  $a_m^{(k,i)}$  be the corresponding activation value.

We can write the  $(mn)$ -th element of  $\nabla_{\mathbf{W}_i} \mathcal{L}(B)$  as the following:

$$\begin{aligned}
[\nabla_{\mathbf{W}_i} \mathcal{L}(B)]_{mn} &= \frac{1}{b} \sum_{(\mathbf{x}, \mathbf{y}) \in B} [\nabla_{\mathbf{W}_i} \ell(\mathbf{x}, \mathbf{y})]_{mn} \\
&= \frac{1}{b} \sum_{k=1}^b a_m^{(k,i-1)} \cdot \frac{\partial \ell^{(k)}}{\partial z_n^{(k,i)}} \\
&= \frac{1}{b} [a_m^{(1,i-1)} a_m^{(2,i-1)} a_m^{(3,i-1)} \dots a_m^{(b,i-1)}] \begin{bmatrix} \frac{\partial \ell^{(1)}}{\partial z_n^{(1,i)}} \\ \frac{\partial \ell^{(2)}}{\partial z_n^{(2,i)}} \\ \frac{\partial \ell^{(3)}}{\partial z_n^{(3,i)}} \\ \vdots \\ \frac{\partial \ell^{(b)}}{\partial z_n^{(b,i)}} \end{bmatrix} \tag{17}
\end{aligned}$$

To compute the entire gradient  $\nabla_{\mathbf{W}_i} \mathcal{L}(B)$ , not just a single element, we can view it as the matrix multiplication

$$b \nabla_{\mathbf{W}_i} \mathcal{L} = \mathbf{A}_{i-1} \mathbf{D}_i, \tag{18}$$

where  $\mathbf{D}_i \in \mathbb{R}^{b \times d_i}$  and the  $k$ -th row denotes  $\delta_i^{(k)}$  i.e., the error at the  $i$ -th layer for the  $k$ -th example in the mini-batch. Each  $\mathbf{D}_i$  is given by

$$\mathbf{D}_i = (\mathbf{D}_{i+1} \mathbf{W}_{i+1}^T) \odot H_i. \tag{19}$$

Equation (19) is the matrix version of (6). The  $k$ -th row of  $H_i \in \mathbb{R}^{b \times d_i}$  denotes  $\mathbf{h}_i^{(k)}$ , and  $\odot$  gives the hadamard product.  $\nabla_{\mathbf{b}_i} \mathcal{L}$  is given by the average of all the rows of  $\mathbf{D}_i$  e.g.

$$[\nabla_{\mathbf{b}_i} \mathcal{L}]_j = \frac{1}{b} \sum_{k=1}^b [\mathbf{D}_i]_{kj}$$

**Full Proof.** Finally we can prove Proposition 2.

*Proof.* We prove Proposition 2 by proving that there exists a non-zero *perturbation* matrix  $\mathbf{P} \in \mathbb{R}^{d_0 \times b}$  such that for a given mini-batch  $B = \{(\mathbf{x}^{(k)}, \mathbf{y}^{(k)})\}_{k=1}^b$ , a corresponding forged mini-batch  $B'$  can be constructed from  $B$  and  $\mathbf{P}$ , where

$$B' = \{(\mathbf{x}^{(k)} + [\mathbf{P}]^k, \mathbf{y}^{(k)})\}_{k=1}^b$$

and  $\nabla_{\mathbf{W}_i} \mathcal{L}(B) = \nabla_{\mathbf{W}_i} \mathcal{L}(B')$  and  $\nabla_{\mathbf{b}_i} \mathcal{L}(B) = \nabla_{\mathbf{b}_i} \mathcal{L}(B')$  holds  $\forall i \in \{1, 2, \dots, L\}$ . The operator  $[.]^k$  returns the  $k$ -th column of the input matrix. The perturbation matrix  $\mathbf{P}$  itself must satisfy the following 2 matrix equations:

$$\begin{cases} \mathbf{P} \mathbf{D}_1 = \mathbf{0} \\ \mathbf{W}_1^T \mathbf{P} = \mathbf{0} \end{cases} \tag{20}$$

Let  $\mathbf{X}' := \mathbf{X} + \mathbf{P}$ , where  $\mathbf{X}' \in \mathbb{R}^{d_0 \times b}$  represents the input matrix of the forged mini-batch  $B'$  and  $\mathbf{X}$  is the input matrix of mini-batch  $B$ , where the  $k$ -th column of  $\mathbf{X}$  and  $\mathbf{X}'$  denote  $\mathbf{x}^{(k)}$  and  $\mathbf{x}'^{(k)} := \mathbf{x}^{(k)} + [\mathbf{P}]^k$  respectively. Considering the first equation  $\mathbf{P} \mathbf{D}_1 = \mathbf{0}$ , if  $\mathbf{P}$  satisfies this equation, then by (18)

$$\begin{aligned}
b \nabla_{\mathbf{W}_1} \mathcal{L}(B') &= \mathbf{X}' \mathbf{D}_1 \\
&= (\mathbf{X} + \mathbf{P}) \mathbf{D}_1 \\
&= \mathbf{X} \mathbf{D}_1 + \mathbf{P} \mathbf{D}_1 \\
&= \mathbf{X} \mathbf{D}_1 = b \nabla_{\mathbf{W}_1} \mathcal{L}(B).
\end{aligned}$$

Satisfying the first equation ensures that the gradient for the first weight matrix  $\mathbf{W}_1$  will match.

Let  $\mathbf{Z}'_1$  be the batched raw logit output of the first layer, i.e.  $\mathbf{Z}'_1 := \mathbf{W}_1^T \mathbf{X}' + \mathbf{B}_1$ . If  $\mathbf{P}$  satisfies the second equation, then

$$\begin{aligned}
\mathbf{Z}'_1 &= \mathbf{W}_1^T \mathbf{X}' + \mathbf{B}_1 = \mathbf{W}_1^T (\mathbf{X} + \mathbf{P}) + \mathbf{B}_1 \\
&= \mathbf{W}_1^T \mathbf{X} + \mathbf{W}_1^T \mathbf{P} + \mathbf{B}_1 \\
&= \mathbf{W}_1^T \mathbf{X} + \mathbf{B}_1 \\
\mathbf{Z}'_1 &= \mathbf{Z}_1 \\
h(\mathbf{Z}'_1) &= h(\mathbf{Z}_1) \\
\mathbf{A}'_1 &= \mathbf{A}_1
\end{aligned} \tag{21}$$

Since  $\mathbf{A}'_1 = \mathbf{A}_1$ , then  $\mathbf{A}'_i = \mathbf{A}_i \forall i \in \{1, 2, \dots, L\}$ . Satisfying the second equation ensures the activations for the first layer as well as all subsequent layers will be the same as that of the original mini-batch. If we use the same label i.e., each  $\mathbf{y}'^{(k)} = \mathbf{y}^{(k)}$ , then, for the  $k$ -th training example in the forged mini-batch, we have that by (21)  $\hat{\mathbf{y}}'^{(k)} = \hat{\mathbf{y}}^{(k)}$ , therefore

$$\begin{aligned}
\delta'^{(k)}_L &= v'(k) \hat{\mathbf{y}}'^{(k)} - \mathbf{y}'^{(k)} \\
&= v^{(k)} \hat{\mathbf{y}}^{(k)} - \mathbf{y}^{(k)} \\
&= \delta^{(k)}_L
\end{aligned} \tag{22}$$

Therefore  $\mathbf{D}'_L = \mathbf{D}_L$ , and by (19) we can show inductively that  $\mathbf{D}'_i = \mathbf{D}_i, \forall i \in \{1, 2, \dots, L\}$ . We have shown the base case  $i = L$ . To show for  $i = L - 1$ , we first recognise that if  $\forall i, A'_i = A_i$ , then  $H'_i = H_i, \forall i$ . By (19) we then have

$$\begin{aligned}
\mathbf{D}'_i &= (\mathbf{D}'_{i+1} \mathbf{W}_{i+1}^T) \odot H'_i \\
&= (\mathbf{D}_{i+1} \mathbf{W}_{i+1}^T) \odot H_i \\
&= \mathbf{D}_i
\end{aligned} \tag{23}$$

As a result,  $\nabla_{\mathbf{b}_i} \mathcal{L}(B') = \nabla_{\mathbf{b}_i} \mathcal{L}(B), \forall i \in \{1, 2, \dots, L\}$ . By (21) and (23), we have that

$$\begin{aligned}
b \nabla_{\mathbf{W}_i} \mathcal{L}(B') &= \mathbf{A}'_{i-1} \mathbf{D}'_i \\
&= \mathbf{A}_{i-1} \mathbf{D}_i \\
&= b \nabla_{\mathbf{W}_i} \mathcal{L}(B)
\end{aligned} \tag{24}$$

As a result  $\nabla_{\mathbf{W}_i} \mathcal{L}(B') = \nabla_{\mathbf{W}_i} \mathcal{L}(B), \forall i \in \{1, 2, \dots, L\}$ . Therefore, if the perturbation matrix  $\mathbf{P}$  satisfies the 2 matrix equations given in (20), then  $B$  and  $B'$  will produce the same gradient.

In order to construct  $\mathbf{P}$ , we first observe that we can write the equations in (20) as  $\mathbf{I}\mathbf{P}\mathbf{D}_1 = \mathbf{0}$  and  $\mathbf{W}_1^T \mathbf{P}\mathbf{I} = \mathbf{0}$ , where  $\mathbf{I}$  is the identity matrix of appropriate shape. We also have, by the “vec trick”, that for any matrices  $A, X, B$  and  $C$  the following identity:

$$AXB = C \iff (B^T \otimes A)\text{vec}(X) = \text{vec}(C),$$

where  $\otimes$  is the Kronecker product, and  $\text{vec}(\cdot)$  returns the vector after stacking all the columns of the input matrix vertically. We can rewrite our two equations as the following two linear systems:

$$\begin{cases} (\mathbf{D}_1^T \otimes \mathbf{I})\text{vec}(\mathbf{P}) = \text{vec}(\mathbf{0}) \\ (\mathbf{I}^T \otimes \mathbf{W}_1^T)\text{vec}(\mathbf{P}) = \text{vec}(\mathbf{0}) \end{cases}$$

The first coefficient matrix  $(\mathbf{D}_1^T \otimes \mathbf{I}) \in \mathbb{R}^{d_1 d_0 \times d_0 b}$ , and the second coefficient matrix  $(\mathbf{I}^T \otimes \mathbf{W}_1^T) \in \mathbb{R}^{d_1 b \times d_0 b}$ , so we can combine them into the single linear system by stacking them vertically:

$$\begin{bmatrix} \mathbf{D}_1^T \otimes \mathbf{I} \\ \mathbf{I}^T \otimes \mathbf{W}_1^T \end{bmatrix} \text{vec}(\mathbf{P}) = \text{vec}(\mathbf{0}) \tag{25}$$

Let  $\mathbf{K} \in \mathbb{R}^{(d_1 d_0 + d_1 b) \times d_0 b}$  be the above coefficient matrix, then the general solution is given by:

$$\text{vec}(\mathbf{P}) = (\mathbf{I} - \mathbf{K}^+ \mathbf{K}) \mathbf{F}, \tag{26}$$

where  $\mathbf{F} \in \mathbb{R}^{d_0 b}$  is an arbitrary matrix, and  $\mathbf{K}^+$  is the psuedo-inverse of  $\mathbf{K}$ .

For the homogenous linear system  $\mathbf{K}\text{vec}(\mathbf{P}) = \text{vec}(\mathbf{0})$ , there are  $d_0 b - \text{rank}(\mathbf{K})$  linearly independent solutions. If  $\mathbf{K}$  is full rank and square, there are no non-trivial solutions. In order to ensure at least 1 set of linearly dependent solutions (e.g. one free variable)  $d_0 b > d_1 d_0 + d_1 b$  must hold. This ensures that  $d_0 b - \text{rank}(\mathbf{K}) \geq 1$ .  $\square$

4) **Proof of Proposition 3:** Before going onto the full proof, we introduce the following lemma.

**Lemma 4.** For any training example  $(\mathbf{x}, \mathbf{y})$ ,  $\sum_{j=1}^n \frac{\partial \ell(\mathbf{x}, \mathbf{y})}{\partial z_j} = 0$ .

*Proof.*

$$\begin{aligned}
\sum_{j=1}^n \frac{\partial \ell}{\partial z_j} &= \sum_{j=1}^n \left( -y_j + s_j \sum_{k=1}^n y_k \right) \\
&= -\sum_{j=1}^n y_j + \sum_{j=1}^n s_j \cdot \sum_{k=1}^n y_k \\
&= -\sum_{j=1}^n y_j + \sum_{k=1}^n y_k \\
&= 0.
\end{aligned} \tag{27}$$

□

**Full Proof.** We can now prove Proposition 3.

*Proof.* Let  $\mathbf{G} = \nabla_{\mathbf{W}} \mathcal{L}(B; \mathbf{W})$ . Finding a batch  $B' = \{(\mathbf{x}'^{(1)}, \mathbf{y}'^{(1)}), (\mathbf{x}'^{(2)}, \mathbf{y}'^{(2)}), \dots, (\mathbf{x}'^{(b)}, \mathbf{y}'^{(b)})\}$  with  $b \geq \text{rank}(\mathbf{G})$ , such that  $\nabla_{\mathbf{W}} \mathcal{L}(B'; \mathbf{W}) = \mathbf{G}$  requires that for every  $(i, j) \in [d] \times [n]$ ,

$$\frac{\partial \ell'^{(1)}}{\partial z_j'^{(1)}} x_i'^{(1)} + \frac{\partial \ell'^{(2)}}{\partial z_j'^{(2)}} x_i'^{(2)} + \dots + \frac{\partial \ell'^{(b)}}{\partial z_j'^{(b)}} x_i'^{(b)} = b \mathbf{G}_{ij}, \tag{28}$$

where each  $\ell'^{(k)} = \ell(\mathbf{x}'^{(k)}, \mathbf{y}'^{(k)})$ , and  $\mathbf{z}'^{(k)} = \mathbf{W}^T \mathbf{x}'^{(k)}$ . We can restate the problem as finding matrices  $\mathbf{X}' \in \mathbb{R}^{d \times b}$  and  $\mathbf{D} \in \mathbb{R}^{b \times n}$  such that

$$\mathbf{X}' \mathbf{D} = b \mathbf{G}, \tag{29}$$

The  $k$ -th column of  $\mathbf{X}'$  represents  $\mathbf{x}'^{(k)}$ , and the  $k$ -th row of  $\mathbf{D}$  represents  $\frac{\partial \ell'^{(k)}}{\partial \mathbf{z}'^{(k)}}$ . From Lemma 4, the elements of every row of  $\mathbf{D}$  must sum to zero. Construct a matrix  $\mathbf{D}$  such that  $\text{rank}(\mathbf{D}) = \text{rank}(\mathbf{G})$ , and the elements of every row of  $\mathbf{D}$  sum to zero. Finding the corresponding  $\mathbf{X}'$  amounts to solving the linear system

$$\mathbf{D}^T \mathbf{x}'_i = b \mathbf{g}_i \tag{30}$$

where  $\mathbf{x}'_i$  and  $\mathbf{g}_i$  are the transposed  $i$ -th row of  $\mathbf{X}'$  and  $\mathbf{G}$  respectively. For each  $i$ , we know that  $\text{rank}(\mathbf{D}^T) = \text{rank}(\mathbf{D}^T | b \mathbf{g}_i)$ , therefore we can be certain that at least one solution exists.

Finally, the batch of examples  $B'$  whose gradient  $\nabla_{\mathbf{W}} \mathcal{L}(B'; \mathbf{W}) = \mathbf{G}$  can be constructed from the matrices  $\mathbf{X}'$  and  $\mathbf{D}$ . For every  $k \in [b]$ ,  $\mathbf{x}'^{(k)}$  is the given by the  $k$ -th column of  $\mathbf{X}'$ , and as shown in Lemma 4, each  $\mathbf{y}'^{(k)} = v^{(k)} \hat{\mathbf{y}}^{(k)} - [\mathbf{D}]_k^T$ , for any constant  $v^{(k)} \in \mathbb{R}$ , and  $[\mathbf{D}]_k$  returns the  $k$ -th row of  $\mathbf{D}$ . □

### B. Brute Force Forging

Real images consist of 256 possible pixel values. Given an image consisting of just 2 pixels (with a single channel), 3 possible classes, and a batch size of 2, this would result in  $\binom{256^2 \times 3}{2} \approx 1.9 \times 10^{10}$  mini-batches. Computing the gradient of and comparing that many mini-batches is not practical; so an evaluation of the brute force approach is not possible when we allow 256 possible values. However, when we consider much smaller values for  $v$ , the number of allowed values, namely just 2 and 3, the task becomes much more feasible. In other words, when  $v = 2$ , pixels may have only the values 0 or 255 i.e., on or off. For  $v = 3$ , pixels may take the values, 0, 127, or 255 i.e., 3 possible values. This drastically reduces the number of mini-batches that we need to search through.

For a given setup i.e., values of  $d, b, v$ , and  $n$ , we run the following experiment:

- 1) Sample a true minibatch  $B$  from the possible  $\binom{v^d \times n}{b}$  number of mini-batches.
- 2) Calculate its gradient  $\nabla_{\theta} \mathcal{L}(B)$ .
- 3) Search through all  $\binom{v^d \times n}{b} - 1$  other mini-batches for a distinct mini-batch that produces the same gradient.

We run this experiment on a logistic regression model, as well as a  $L = 2$  fully connected neural network with 10 hidden units and ReLU activation function. We additionally fix  $d = 4$  and  $n = 3$ . Table IV summarises our results.

### C. Comparison of Data Forging Attacks

In Figure 6, we plot the performance of both Thudi et al. [23] and Zhang et al. [29]'s data forging attacks, for both LeNet/MNIST and VGGmini/CIFAR10 execution traces.

	$b = 1$	$b = 2$	$b = 3$	$b = 4$	$b = 5$
$v = 2$	$\text{X}(48)$	$\text{X}(1128)$	$\text{X}(17,296)$	$\text{X}(194,580)$	$\text{X}(1,712,304)$
$v = 3$	$\text{X}(243)$	$\text{X}(29,403)$	$\text{X}(2,362,041)$	$\text{?}(141,722,460)$	$\text{?}(6.77 \times 10^9)$
$v = 4$	$\text{X}(768)$	$\text{X}(294,528)$	$\text{?}(75,202,816)$	$\text{?}(1.43 \times 10^{10})$	$\text{?}(2.2 \times 10^{12})$
$v = 5$	$\text{X}(1,875)$	$\text{X}(1,756,875)$	$\text{?}(1.1 \times 10^9)$	$\text{?}(5.13 \times 10^{11})$	$\text{?}(1.92 \times 10^{14})$
$v = 6$	$\text{X}(3,888)$	$\text{X}(7,556,328)$	$\text{?}(9.79 \times 10^9)$	$\text{?}(9.51 \times 10^{12})$	$\text{?}(7.38 \times 10^{15})$

TABLE IV: For increasingly large values of  $v$  and  $b$  ( $d$  and  $n$  are fixed to  $d = 4$  and  $n = 3$ ), we report, after searching through all the possible mini-batches, whose total number is given in brackets, whether a forged mini-batch that produced the same gradient was found. In every case, we did not find one after an exhaustive search. We give a  $\text{?}$  in those setting where we did not conduct a search, due to the large number of possible mini-batches.

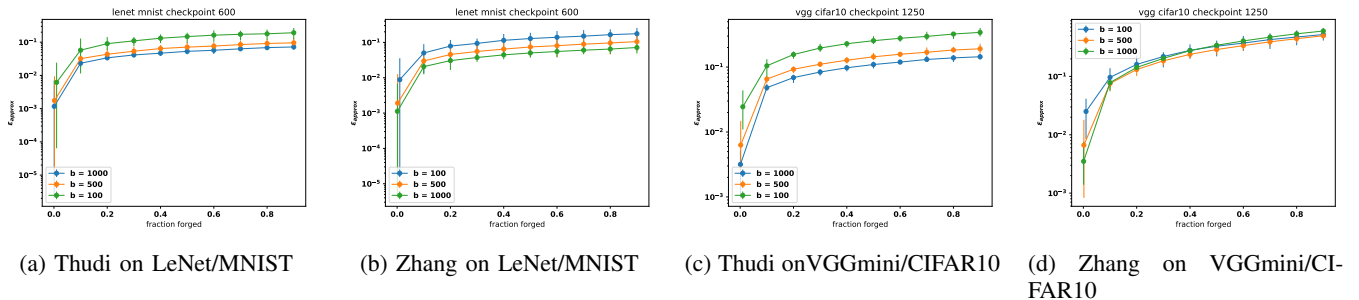


Fig. 6: We plot the average approximation error of both Thudi et al.'s [23] and Zhang et al.'s [29] attack (over several runs), as well as the min and max observed approximation error for different batch sizes and increasing forging fractions. We see both produce similar performance.